Nonlinear perturbation theory with halo bias and redshift-space distortions via the Lagrangian picture

Takahiko Matsubara*

Department of Physics, Nagoya University, Chikusa, Nagoya, 464-8602, Japan

(Dated: November 13, 2008)

The nonlinear perturbation theory of gravitational instability is extended to include effects of both biasing and redshift-space distortions, which are inevitable in predicting observable quantities in galaxy surveys. Weakly nonlinear effects in galaxy clustering on large scales recently attracted a great interest, since the precise determination of scales of baryon acoustic oscillations is crucial to investigate the nature of dark energy by galaxy surveys. We find that a local Lagrangian bias and redshift-space distortions are naturally incorporated in our formalism of perturbation theory with a resummation technique via the Lagrangian picture. Our formalism is applicable to any biasing scheme which is local in Lagrangian space, including the halo bias as a special case. Weakly nonlinear effects on halo clustering in redshift space are analytically given. We assume only a fundamental idea of the halo model: haloes form according to the extended Press–Schechter theory, and the spatial distributions are locally biased in Lagrangian space. There is no need for assuming the spherical collapse model to follow the dynamical evolution, which is additionally assumed in standard halo prescriptions. One-loop corrections to the power spectrum and correlation function of haloes in redshift space are explicitly derived and presented. Instead of relying on expensive numerical simulations, our approach provides an analytic way of investigating the weakly nonlinear effects, simultaneously including the nonlinear biasing and nonlinear redshift-space distortions. Nonlinearity introduces a weak scale dependence in the halo bias. The scale dependence is a smooth function in Fourier space, and the bias does not critically change the feature of baryon acoustic oscillations in the power spectrum. The same feature in the correlation function is less affected by nonlinear effects of biasing.

I. INTRODUCTION

The nonlinear perturbation theory of gravitational instability has recently attracted renewed interest. As precision measurements of the large-scale structure of the universe become possible, theoretically accurate modeling is essential to interpret the observational data. It is recognized that the linear perturbation theory is not satisfactory for this purpose. The importance of nonlinear perturbation theory resides in the era of precision cosmology.

A strong motivation for developing the perturbation theory is to model the baryon acoustic oscillations (BAOs) imprinted in the large-scale structure. Acoustic waves which propagate in the baryon-photon plasma of the early universe freeze out at the recombination epoch, and the sound horizon at that epoch is imprinted in spatial fluctuations of photons and baryons [1, 2]. The BAOs provide a standard ruler [3] to geometrically investigate the expansion history of the Universe [4]. The dark energy component is efficiently constrained by galaxy surveys of an intermediate- to high-redshift universe [5, 6]. Using the BAOs as a standard ruler, large galaxy surveys are expected to provide a robust, promising way of constraining the nature of dark energy [7, 8]. Recent observations of BAOs in modern galaxy surveys [9] prove the method works well.

Even though the BAO scale is quite large $\sim 100\,h^{-1}$Mpc, detailed structure of BAOs in galaxy clustering is affected by gravitationally nonlinear evolution after the recombination epoch. The BAO signature in the power spectrum or in the correlation function is deformed by nonlinearity in a lower redshift universe where realistic galaxy surveys are possible [10, 11, 12, 13, 14].

In galaxy redshift surveys, the clustering of dark matter is not directly observable. There are two major sources in the difference between the clustering pattern of dark matter and that of galaxies: galaxy biasing and redshift-space distortions. The spatial pattern of galaxy distribution is not necessarily the same as that of dark matter, and the galaxies are biased tracers of mass [15, 16]. The redshift of a galaxy does not purely reflect the Hubble flow, and the Doppler shift by a peculiar velocity is inevitably added. Thus the spatial pattern of clustering of galaxies is distorted in redshift space [17, 18]. In the linear regime, the power spectrum of biased objects $P_{\rm obj}(k)$ is usually assumed to be proportional to that of mass $P_{\rm m}(k)$ in real space: $P_{\rm obj}(k) = b^2 P_{\rm m}(k)$, and there is a theoretical reason, which is known as "the local bias theorem" [19, 20]. Assuming linear dynamics, a linear bias, and a linear velocity field, the power spectrum of biased objects in redshift space is given by [18]

$$P_{\rm g}^{\rm (s)}(\boldsymbol{k}) = b^2 \left(1 + \beta \mu^2\right)^2 P_{\rm m}(k), \tag{1}$$

where b is the linear bias factor between galaxies and mass, $\beta \simeq \Omega_{\rm m}^{0.6}/b$, and $P_{\rm m}(k)$ is the power spectrum of mass in real space.

The linear formula of Eq. (1) applies only when the redshift is large enough, or when the wave number k is small enough. However, the linear formula in redshift space is not sufficiently accurate for typical redshift surveys [21]. Extending the linear formula of Eq. (1) to include nonlinear effects

*Electronic address: taka@a.phys.nagoya-u.ac.jp

is far from trivial. A straightforward application of the nonlinear perturbation theory [22, 23, 24, 25] with a local biasing scheme [26] has been studied so far [27, 28, 29, 30]. In the local biasing scheme, the number density of biased objects is a local function of the smoothed density field of mass in Eulerian space. This scheme seems to work as long as the tree-level perturbation theory is adopted [31]. However, when loop corrections are considered, there appears a conceptual problem in the local biasing scheme. It turns out that the one-loop corrections, even on large scales, strongly depend on the artificial smoothing scale [27]. In Ref. [29], a way to remove the dependence on the smoothing scale by renormalizing bias parameters is proposed. While this could be a solution to phenomenologically represent the power spectrum of biased objects [32], it is not guaranteed that the procedure actually reflects the physical nature of biasing, since the biasing is more or less a nonlocal process.

It is true that the biasing is difficult to be included exactly in an analytic framework, since the galaxy formation is a highly nonlinear process. The next best thing is to find a good analytic model. In this respect, a plausible model is provided by a halo approach [33, 34, 35, 36, 37, 38, 39, 40, 41], which is based on the extended Press and Schechter (PS) model [42, 43]. In this approach, the galaxy biasing is described through two steps. In the first step, the formation and clustering of dark matter haloes are analytically modeled by using the extended PS model. The spherical collapse model is combined to include the gravitational evolution of halo positions. In the second step, the distribution of dark matter or galaxies within haloes is empirically modeled with a number of assumptions [37, 38, 39, 40, 41, 44], which include complicated physics such as gas cooling, star formation, feedback effects from supernovae, and so forth [45].

While the second step involves many parameters which should be fitted by observations or simulations, the first step is theoretically less uncertain because of its purely gravitational nature. On large scales, the second step is not important and the power spectrum of nonlinear objects is approximately the same as that of haloes. Therefore, determining the power spectrum of haloes is an important step toward understanding the nonlinear structure formation and biasing. In the usual halo approach, the halo clustering is modeled by linear dynamics and linear bias factors [33, 37, 38, 39, 40]. Recently, an attempt to incorporate the halo bias with nonlinear perturbation theory in a framework of local biasing scheme has been made [30]. There still remains conceptual arbitrariness in the latter formulation, mainly because the halo bias is intrinsically nonlocal in Eulerian space and does not fit well into the local Eulerian biasing scheme. From the construction, the halo bias is local in Lagrangian space [33], and is therefore nonlocal in Eulerian space, because positions of mass and biased objects are displaced by dynamical evolution.

In this paper, a natural approach to incorporate the halo bias and redshift-space distortions with nonlinear perturbation theory is newly developed. To account for the locality of halo bias in Lagrangian space, our formulation is based on the Lagrangian perturbation theory (LPT) [46], instead of the standard Eulerian perturbation theory (EPT). In the original halo approach, the spherical collapse model is adopted to take into account the dynamical evolution in Eulerian space. However, the dynamical evolution of haloes is more naturally described in the Lagrangian picture [47]. It is not straightforward to obtain an analytically useful formalism which combines the LPT and the halo approach. A main obstacle is that the observable quantities reside in Eulerian space, while the calculations in LPT directly give Lagrangian quantities. In paper I [48], a new approach is developed to overcome this point, partially expanding the Lagrangian variables in Eulerian space. The resulting expression contains an infinite series of perturbations in terms of the EPT, and this approach offers a simplified technique of resumming cosmological perturbations, such as done in renormalized perturbation theory and its variants [49, 50]. While our technique is not suitable enough to describe the fully nonlinear regime which other renormalization techniques aim at, we have shown in paper I that our technique is accurate enough in the quasilinear regime, and most importantly, predictions in redshift space are straightforward. To date, our technique offers the only way of obtaining resummed power spectra in redshift space. In this paper, we show that the local Lagrangian bias, including the halo bias, is also straightforward to be incorporated in the approach of paper I, on top of the redshift-space distortions. The local Lagrangian biasing scheme is not equivalent to the local Eulerian biasing scheme, and the conceptual problem about the strong dependence on smoothing scales which appears in the local Eulerian biasing scheme described above is not present in our Lagrangian approach.

The rest of the paper is organized as follows. In Sec. II, our basic formalism is described. This formalism is applicable not only to the halo bias but also to a local Lagrangian bias in general. Linear and one-loop results are presented. In this general theory, we have parameters which are related to the Lagrangian biasing scheme. In Sec. III, those Lagrangian bias parameters are calculated from the fundamental concept of the halo model. Effects of halo bias and redshift-space distortions on BAO scales are demonstrated both in the power spectrum and in the correlation function. Our conclusions are summarized in Sec. IV. In the Appendix, details of one-loop calculations in our framework are outlined.

II. LOCAL LAGRANGIAN BIAS

A. Nonlinear power spectrum with a local Lagrangian bias

In this section, we develop a method to track nonlinear evolution of the Lagrangian bias. Our method in this section is not restricted to the halo bias model, and is applicable to any bias defined by a local function of linear density field in Lagrangian space.

In the Lagrangian approach to track dynamical evolution of cosmological density fields, a set of each trajectory of a mass element, $x(q, t)$, where q are initial Lagrangian coordinates, describes the whole property of the density field. A displace-

ment field $\mathbf{\Psi}(\boldsymbol{q}, t)$ is defined by

$$\boldsymbol{x}(\boldsymbol{q}, t) = \boldsymbol{q} + \mathbf{\Psi}(\boldsymbol{q}, t), \tag{2}$$

and is considered as a fundamental variable of the mass density field. Since the initial mass density field is sufficiently uniform, the Eulerian mass density field $\rho_\mathrm{m}(\boldsymbol{x}, t)$ at any given time t satisfies the continuity relation,

$$\rho_\mathrm{m}(\boldsymbol{x}, t)\, d^3 x = \bar{\rho}_\mathrm{m}\, d^3 q, \tag{3}$$

where $\bar{\rho}_\mathrm{m}$ is the global mean density of mass.

On the other hand, the fluid elements in which biased objects such as haloes reside are not uniformly distributed in Lagrangian space. Therefore, the continuity relation between the Eulerian density field of the biased objects, $\rho_\mathrm{obj}^\mathrm{E}(\boldsymbol{x}, t)$, and corresponding Lagrangian density field, $\rho_\mathrm{obj}^\mathrm{L}(\boldsymbol{q})$, is given by

$$\rho_\mathrm{obj}^\mathrm{E}(\boldsymbol{x}, t)\, d^3 x = \rho_\mathrm{obj}^\mathrm{L}(\boldsymbol{q})\, d^3 q. \tag{4}$$

The density field $\rho_\mathrm{obj}^\mathrm{L}(\boldsymbol{q})$ represents the initial distribution of locations where biased objects form later. Since the formation of nonlinear structure is too complex to be analytically described from the first principle, the initial density field $\rho_\mathrm{obj}^\mathrm{L}(\boldsymbol{q})$ of biased objects should be given by a good model of nonlinear structure formation, such as the halo model.

In this paper, we assume locality of the bias in Lagrangian space: the Lagrangian density field $\rho_\mathrm{obj}^\mathrm{L}(\boldsymbol{q})$ is assumed to be a function of a smoothed linear overdensity at the same Lagrangian position,

$$\delta_R(\boldsymbol{q}) = \int d^3 q'\, W_R(|\boldsymbol{q} - \boldsymbol{q}'|)\, \delta_\mathrm{L}(\boldsymbol{q}'), \tag{5}$$

where W_R is a smoothing kernel of size R, and $\delta_\mathrm{L}(\boldsymbol{q})$ is the (unsmoothed) linear overdensity. We call such biasing scheme a "local Lagrangian bias" in this paper. As we will show in the next section, the halo bias [33] is actually a special case of local Lagrangian bias. Another example of the local Lagrangian bias is the peak bias with the approximation of peak-background split [16, 34, 51]. The locality of bias in Lagrangian space does not mean locality in Eulerian space, because of evolutionary effects. Therefore our biasing scheme does not fall into the category of the local biasing scheme in a usual context of EPT. The local Lagrangian bias is nonlocal in Eulerian space.

Thus, we introduce a Lagrangian bias function $F(\delta)$ by

$$\rho_\mathrm{obj}^\mathrm{L}(\boldsymbol{q}) = \bar{\rho}_\mathrm{obj}\, F[\delta_R(\boldsymbol{q})], \tag{6}$$

where $\bar{\rho}_\mathrm{obj}$ is the comoving mean density of the biased objects, which is common in Lagrangian space and in Eulerian space. This function has the following property:

$$\langle F(\delta_R) \rangle = 1. \tag{7}$$

Equation (4) is equivalent to the following equation:

$$\rho_\mathrm{obj}^\mathrm{E}(\boldsymbol{x}) = \bar{\rho}_\mathrm{obj} \int d^3 q\, F[\delta_R(\boldsymbol{q})]\, \delta_\mathrm{D}^3[\boldsymbol{x} - \boldsymbol{q} - \mathbf{\Psi}(\boldsymbol{q})], \tag{8}$$

where δ_D^3 is 3-dimensional Dirac's delta function, and we suppress the time-dependence for notational simplicity. Using the Fourier transform of this equation, we obtain an expression of the power spectrum of biased objects in Eulerian space,

$$P_\mathrm{obj}(\boldsymbol{k}) = \int d^3 q\, e^{-i\boldsymbol{k}\cdot\boldsymbol{q}} \left[\int \frac{d\lambda_1}{2\pi} \frac{d\lambda_2}{2\pi} \tilde{F}(\lambda_1)\tilde{F}(\lambda_2) \right.$$
$$\left. \times \left\langle e^{i[\lambda_1 \delta_R(\boldsymbol{q}_1) + \lambda_2 \delta_R(\boldsymbol{q}_2)] - i\boldsymbol{k}\cdot[\mathbf{\Psi}(\boldsymbol{q}_1) - \mathbf{\Psi}(\boldsymbol{q}_2)]} \right\rangle - 1 \right], \tag{9}$$

where $\tilde{F}(\lambda)$ is the Fourier transform of $F(\delta)$ and $\boldsymbol{q} = \boldsymbol{q}_1 - \boldsymbol{q}_2$. The quantity in the ensemble average $\langle \cdots \rangle$ in the above equation is a function of only $\boldsymbol{q}$ because of translational invariance. In the absence of bias, $F = 1$ and $\tilde{F}(\lambda) = 2\pi\delta_\mathrm{D}(\lambda)$, the Eq. (9) reduces to a known expression [52]. We do not assume rotational invariance for allowing our analysis to include redshift-space clustering. Our convention of the power spectrum is given by

$$\left\langle \tilde{\delta}_\mathrm{obj}(\boldsymbol{k})\tilde{\delta}_\mathrm{obj}(\boldsymbol{k}') \right\rangle = (2\pi)^3 \delta_\mathrm{D}^3(\boldsymbol{k} + \boldsymbol{k}') P_\mathrm{obj}(\boldsymbol{k}), \tag{10}$$

where

$$\tilde{\delta}_\mathrm{obj}(\boldsymbol{k}) = \int d^3 x\, e^{-i\boldsymbol{k}\cdot\boldsymbol{x}} \left[\frac{\rho_\mathrm{obj}^\mathrm{E}(\boldsymbol{x})}{\bar{\rho}_\mathrm{obj}} - 1 \right]. \tag{11}$$

Similarly, the linear power spectrum $P_\mathrm{L}(k)$ is defined by a similar equation to Eq. (10) and a Fourier transform of $\delta_\mathrm{L}(\boldsymbol{q})$.

The expression of Eq. (9) has a form that we can apply to the cumulant expansion theorem [53]

$$\langle e^{-iX} \rangle = \exp\left[\sum_{N=1}^{\infty} \frac{(-i)^N}{N!} \langle X^N \rangle_\mathrm{c} \right], \tag{12}$$

where $\langle X^N \rangle_\mathrm{c}$ denotes a cumulant of a random variable X [25]. The corresponding factor in Eq. (9) thus reduces to

$$\left\langle e^{i[\lambda_1 \delta_R(\boldsymbol{q}_1) + \lambda_2 \delta_R(\boldsymbol{q}_2)] - i\boldsymbol{k}\cdot[\mathbf{\Psi}(\boldsymbol{q}_1) - \mathbf{\Psi}(\boldsymbol{q}_2)]} \right\rangle$$
$$= \exp\left[\sum_{n_1+n_2+m_1+m_2 \geq 1} \frac{i^{n_1+n_2+m_1+m_2}}{n_1! n_2! m_1! m_2!} \lambda_1{}^{n_1} \lambda_2{}^{n_2} B_{m_1 m_2}^{n_1 n_2}(\boldsymbol{k}, \boldsymbol{q}) \right], \tag{13}$$

where the multinomial theorem is used, and

$$B_{m_1 m_2}^{n_1 n_2}(\boldsymbol{k}, \boldsymbol{q}) = (-1)^{m_1}$$
$$\times \langle [\delta_R(\boldsymbol{q}_1)]^{n_1} [\delta_R(\boldsymbol{q}_2)]^{n_2} [\boldsymbol{k} \cdot \mathbf{\Psi}(\boldsymbol{q}_1)]^{m_1} [\boldsymbol{k} \cdot \mathbf{\Psi}(\boldsymbol{q}_2)]^{m_2} \rangle_\mathrm{c}. \tag{14}$$

The translational invariance and the parity symmetry imply the following identities:

$$B_{m_1 m_2}^{n_1 n_2}(\boldsymbol{k}, \boldsymbol{q}) = (-1)^{m_1+m_2} B_{m_2 m_1}^{n_2 n_1}(\boldsymbol{k}, -\boldsymbol{q}), \tag{15}$$
$$= (-1)^{m_1+m_2} B_{m_1 m_2}^{n_1 n_2}(\boldsymbol{k}, -\boldsymbol{q}), \tag{16}$$

and therefore Eq. (14) is symmetric with respect to its indices:

$$B_{m_1 m_2}^{n_1 n_2}(\boldsymbol{k}, \boldsymbol{q}) = B_{m_2 m_1}^{n_2 n_1}(\boldsymbol{k}, \boldsymbol{q}). \tag{17}$$

When the initial density field is random Gaussian, which is assumed throughout this paper, the Equation (14) of $m_1 = m_2 = 0$ survives only when $n_1 + n_2 = 2$:

$$B_{00}^{n_1 n_2}(\boldsymbol{k}, \boldsymbol{q}) = \begin{cases} \xi_R(|\boldsymbol{q}|), & n_1 = n_2 = 1, \\ \sigma_R^2, & (n_1 = 2, n_2 = 0) \text{ or } (n_1 = 0, n_2 = 2), \\ 0, & \text{otherwise}, \end{cases}$$

(18)

where $\sigma_R^2 = \xi_R(0)$, and $\xi_R(q)$ is the smoothed linear correlation function of the linear density field,

$$\xi_R(q) = \int \frac{k^2 dk}{2\pi^2} j_0(kq) W^2(kR) P_L(k),$$

(19)

where $j_0(x) = x^{-1} \sin x$ is the spherical Bessel function of zeroth order, and

$$W(kR) = 4\pi \int x^2 dx j_0(kx) W_R(x)$$

(20)

is the window function of the smoothing kernel. For the equation (14) of $n_1 = n_2 = 0$, we have

$$B_{m_1 m_2}^{00}(\boldsymbol{k}, \boldsymbol{q})$$
$$= \begin{cases} A_{2m}(\boldsymbol{k}), & (m_1 = 2m, m_2 = 0) \text{ or } (m_1 = 0, m_2 = 2m), \\ B_{m_1 m_2}(\boldsymbol{k}, \boldsymbol{q}), & m_1 \geq 1 \text{ and } m_2 \geq 1, \\ 0, & \text{otherwise}, \end{cases}$$

(21)

where m is a positive integer, and

$$A_{2m}(\boldsymbol{k}) \equiv \left\langle [\boldsymbol{k} \cdot \boldsymbol{\Psi}(0)]^{2m} \right\rangle_c,$$

(22)

$$B_{m_1 m_2}(\boldsymbol{k}, \boldsymbol{q}) \equiv (-1)^{m_1} \left\langle [\boldsymbol{k} \cdot \boldsymbol{\Psi}(\boldsymbol{q}_1)]^{m_1} [\boldsymbol{k} \cdot \boldsymbol{\Psi}(\boldsymbol{q}_2)]^{m_2} \right\rangle_c.$$

(23)

Using the above properties and quantities, and substituting Eq. (13) into Eq. (9), we obtain an expression,

$$P_{\text{obj}}(\boldsymbol{k}) = \exp\left[2 \sum_{m=1}^{\infty} \frac{(-1)^m}{(2m)!} A_{2m}(\boldsymbol{k})\right] \int d^3 q\, e^{-i\boldsymbol{k}\cdot\boldsymbol{q}} \exp\left[\sum_{m_1, m_2 \geq 1}^{\infty} \frac{i^{m_1 + m_2}}{m_1! m_2!} B_{m_1 m_2}(\boldsymbol{k}, \boldsymbol{q})\right]$$
$$\times \int_{-\infty}^{\infty} \frac{d\lambda_1}{2\pi} \frac{d\lambda_2}{2\pi} \tilde{F}(\lambda_1) \tilde{F}(\lambda_2) e^{-\lambda_1^2 \sigma_R^2/2 - \lambda_2^2 \sigma_R^2/2} \exp\left[-\lambda_1 \lambda_2 \xi_R(|\boldsymbol{q}|) + \sum_{n_1+n_2 \geq 1}^{\infty} \sum_{m_1+m_2 \geq 1}^{\infty} \frac{i^{n_1+n_2+m_1+m_2}}{n_1! n_1! m_1! m_2!} \lambda_1^{n_1} \lambda_2^{n_2} B_{m_1 m_2}^{n_1 n_2}(\boldsymbol{k}, \boldsymbol{q})\right]$$
$$- (2\pi)^3 \delta_D^3(\boldsymbol{k}). \quad (24)$$

So far the expression is formal and holds even on strongly nonlinear scales. Gravitational nonlinear effects on the matter distribution and on the bias are all included in the cumulants of Eq. (14). When the objects are unbiased, $F(\delta) = 1$, $\tilde{F}(\lambda) = 2\pi\delta_D(\lambda)$, the second line of Eq. (24) simply reduces to unity, and the expression is equivalent to the one that was previously derived in Eq. (8) of paper I [48]. In the work of paper I, we applied the LPT to evaluate the cumulants of Eq. (14) when $n_1 = n_2 = 0$, and showed that expanding only the exponential factor in the integrand and keeping the exponential prefactor result in partial resummation of Eulerian perturbations, which improves the standard EPT in quasi-linear regime. This is justified by the fact that the exponential prefactor consists only of cumulants of the displacement field at a single point, while the remaining exponential factor consists of cumulants at two points separated by $|\boldsymbol{q}| \sim |\boldsymbol{k}|^{-1}$. The latter cumulants are small enough in a large-scale limit, $|\boldsymbol{k}| \to 0$. When the exponential prefactor is expanded as well, this approach gives equivalent results to the standard EPT. Evaluation of the cumulants in redshift space is straightforward in the framework of LPT.

In the presence of Lagrangian biasing, a similar technique can be adopted. In the integrand of λ_1 and λ_2, we expand the last exponential factor, keeping the exponential prefactor which involves σ_R^2. In a large-scale limit, $\sigma_R^2 \gg \xi_R(|\boldsymbol{q}|)$ because $|\boldsymbol{q}|$ is large, and $\sigma_R^2 \gg B_{m_1 m_2}^{n_1 n_2}$ ($m_1 + m_2 \geq 1$) because

$|\boldsymbol{k}|$ is small. Therefore, it is desirable to keep the exponential prefactor in the integrand of λ's. Expanding the last exponential factor, the integrals of λ's can be performed as

$$\int_{-\infty}^{\infty} \frac{d\lambda}{2\pi} \tilde{F}(\lambda) e^{-\lambda^2 \sigma_R^2/2} (i\lambda)^n = \frac{1}{\sqrt{2\pi}\,\sigma_R} \int_{-\infty}^{\infty} d\delta\, e^{-\delta^2/2\sigma_R^2} \frac{d^n F}{d\delta^n}$$
$$\equiv \left\langle F^{(n)} \right\rangle.$$

(25)

The right-hand side (RHS) of Eq. (25) corresponds to the expectation value of derivatives of F. In the following, we use notations such as $\langle F' \rangle$, $\langle F'' \rangle$ for $n = 1, 2$, respectively, to represent the above integral. The local Lagrangian bias is fully characterized by a series of these parameters $\langle F^{(n)} \rangle$, which we call local Lagrangian bias parameters.

The exponential prefactor in Eq. (24) corresponds to the characteristic function of the one-point distribution of displacement field. In fact, from Eqs. (12) and (22) and parity property, $A_{2m+1} = 0$, we have

$$\exp\left[2 \sum_{m=1}^{\infty} \frac{(-1)^m}{(2m)!} A_{2m}(\boldsymbol{k})\right] = \left| \left\langle e^{-i\boldsymbol{k}\cdot\boldsymbol{\Psi}} \right\rangle \right|^2.$$

(26)

Evaluation of the above characteristic function of the RHS requires the fully nonlinear dynamics. In this paper, the exponent of the LHS is evaluated by adopting the perturbation theory.

Before closing this subsection, we comment on the role of smoothing radius R. In the local Lagrangian biasing scheme with peak-background split, the number density of biased objects is spatially modulated by the linearly extrapolated background density field in Lagrangian space. The large-scale clustering of biased objects should not depend on the artificial choice of smoothing radius R to define the background field. In fact, in the case of halo bias, it is explicitly shown that $\langle F^{(n)} \rangle$ is independent on R. In our derivation, we have used an approximation $\sigma_R^2 \gg \xi_R(|\boldsymbol{q}|)$, which means our equations are valid on larger scales than the smoothing radius of the Lagrangian bias: $k \ll R^{-1}$. In particular, the smoothing kernel $W(kR)$ in final expressions of our perturbation theory is replaced by unity, for consistency with our approximation in the first place.

B. Biased power spectrum from Lagrangian perturbation theory

We evaluate the general Eq. (24) via the LPT as outlined in the previous section. Details of derivations by the one-loop perturbation theory are given in the Appendix. In this subsection, we summarize basic assumptions made in the derivations.

As explained above, we need to evaluate the cumulants $B_{m_1 m_2}^{n_1 n_2}(\boldsymbol{k}, \boldsymbol{q})$ of Eq. (14). In LPT, the displacement field is expanded as a perturbative series,

$$\boldsymbol{\Psi} = \boldsymbol{\Psi}^{(1)} + \boldsymbol{\Psi}^{(2)} + \boldsymbol{\Psi}^{(3)} + \cdots, \tag{27}$$

where $\boldsymbol{\Psi}^{(n)}$ is given by integrations over nth product of linear density contrast δ_{L} with kernels as in Eq. (A2). By means of LPT, the cumulant of Eq. (14) reduces to an infinite sum over cumulants of linear density contrast, which are straightforwardly given by the linear power spectrum. On large scales where $|\boldsymbol{k}| \ll |\boldsymbol{\Psi}|$, contributions from higher-order perturbations in Eq. (27) are small enough, and one can truncate the series. In the perturbation theory, a consistent manner of truncation is given by a loop-expansion [25] to obtain a nonlinear power spectrum. For Gaussian initial conditions, the loop expansion is equivalent to the series expansion in terms of the linear power spectrum $P_{\mathrm{L}}(k)$.

The treatment of nonlinear redshift-space distortions is simpler in LPT than that in EPT as shown in paper I [48]. The displacement field in redshift space $\boldsymbol{\Psi}^{\mathrm{s}}$ is given by

$$\boldsymbol{\Psi}^{\mathrm{s}} = \boldsymbol{\Psi} + \frac{\hat{\boldsymbol{z}} \cdot \dot{\boldsymbol{\Psi}}}{H} \hat{\boldsymbol{z}}, \tag{28}$$

where $\boldsymbol{\Psi}$ is the displacement field in real space, a dot denotes the derivative with respect to the cosmic time t, $\hat{\boldsymbol{z}}$ is a unit vector along the line of sight, $H = \dot{a}/a$ is the time-dependent Hubble parameter, and $a(t)$ is the scale factor. The relation between displacement fields in Eq. (28) is exactly linear even in the nonlinear regime. In contrast, the redshift-space distortions of Eulerian variables are given by nonlinear transformations. This is a reason why nonlinear redshift-space distortions are easier to handle in LPT than that in EPT.

The time dependence of each perturbative term in Eq. (27) is approximately given by $\boldsymbol{\Psi}^{(n)} \propto D^n$, where $D(t)$ is the linear growth rate. This relation is exact in the Einstein-de Sitter model, and approximately holds in general cosmology [25, 54]. We also apply the distant-observer approximation in which the line of sight $\hat{\boldsymbol{z}}$ is fixed. The latter approximation is commonly used in analyses of redshift-space distortions and valid as long as the redshift surveys are deep enough so that clustering scales of interest is smaller than distances between the observer and galaxies [55]. With those approximations, order-by-order linear transformations of displacement fields become particularly simple: $\boldsymbol{\Psi}^{\mathrm{s}(n)} = R^{(n)} \boldsymbol{\Psi}^{(n)}$, where $R^{(n)}$ is a 3×3 matrix whose components are given by Eq. (A7).

Keeping the one-loop LPT exact, the integrand of Eq. (24) turns out to be a strongly oscillating function of $\boldsymbol{q}$. It seems extremely difficult to numerically evaluate such integral. Instead, we further expand and truncate the exponential factors in the integrand at the one-loop level as explained in the previous subsection. This means that our result is not exact at one-loop LPT, while the neglected terms are of order $O[P_{\mathrm{L}}(k)]^3$, which are two- or or higher-loop contributions in terms of Eulerian perturbations. Not expanding the exponential prefactor improves the standard EPT as shown in paper I.

C. The linear power spectrum in real space and in redshift space

Expanding Eq. (24) and keeping only linear terms in $P_{\mathrm{L}}(k)$, we obtain the biased power spectrum in linear perturbation theory. The result in real space is simply given by a linear term of Eq. (A69) with a substitution $f = 0$,

$$P_{\mathrm{obj}}(k) = (1 + \langle F' \rangle)^2 P_{\mathrm{L}}(k). \tag{29}$$

Since the mass power spectrum is given by $P_{\mathrm{m}}(k) = P_{\mathrm{L}}(k)$ in linear theory, the linear bias factor b, which is defined by

$$P_{\mathrm{obj}}(k) = b^2 P_{\mathrm{m}}(k), \tag{30}$$

is scale-independent:

$$b = 1 + \langle F' \rangle, \tag{31}$$

i.e., b does not depend on k in a large-scale limit. In the original halo approach, it is derived that the Eulerian linear bias factor is given by the Lagrangian linear bias factor plus unity by using a spherical collapse model [33, 34, 36]. The result of Eq. (31), which is derived without assuming spherical collapse, is consistent to that approach. In this sense, the factor $\langle F' \rangle$ corresponds to a Lagrangian linear bias factor.

It is interesting to notice that the linear bias should be scale-independent in this limit, for any nonlinear function of F: in linear perturbation theory, scale dependence cannot be produced by any form of local Lagrangian bias. This result can be considered as a generalization of the "local bias theorem" [19, 20], which states that the linear bias factor of local *Eulerian* bias for sufficiently small k is scale independent. The constancy of the linear bias factor is now proven even for the

local *Lagrangian* bias, which is nonlocal in Eulerian space. It is known that the additional constant term arises from small-scale inaccuracies of the linear power spectrum, and the general asymptotic form of biased power spectrum is given by $P_{\mathrm{obj}}(k) = b^2 P_{\mathrm{m}}(k) + c$ in a large-scale limit [20].

The corresponding linear result in redshift space is given by a linear term of Eq. (A69),

$$P_{\mathrm{obj}}^{(\mathrm{s})}(\boldsymbol{k}) = \left(1 + \langle F' \rangle + f\mu^2\right)^2 P_{\mathrm{L}}(k), \tag{32}$$

where $\mu = \hat{\boldsymbol{z}} \cdot \boldsymbol{k}/k$ is the direction cosine of the wavevector $\boldsymbol{k}$ with respect to the line of sight $\hat{\boldsymbol{z}}$, $f = d\ln D/d\ln a = (HD)^{-1}\dot{D}$ is the logarithmic derivative of the linear growth rate $D(t)$. This result is equivalent to the Kaiser's formula [18]

$$P_{\mathrm{obj}}^{(\mathrm{s})}(\boldsymbol{k}) = b^2 \left(1 + \beta\mu^2\right)^2 P_{\mathrm{m}}(k), \tag{33}$$

where the linear bias factor b is given by Eq. (31) and $\beta = f/b$ is the redshift-space distortion parameter. Again, it is interesting to notice that we have derived the Kaiser's formula in the presence of any nonlinear local bias in Lagrangian space: the Kaiser's formula with a scale-independent bias is a general consequence of a large-scale limit even in this framework.

D. One-loop corrections to the biased power spectrum

The formal expression of Eq. (24) is evaluated by applying the LPT. The derivation of one-loop corrections to the power spectrum is detailed in the Appendix. The power spectrum in real space with one-loop corrections is given by putting $f = 0$ in Eq. (A69). The result is

$$
\begin{aligned}
P_{\mathrm{obj}}(k) = \exp&\left[-(k/k_{\mathrm{NL}})^2\right] \\
\times \Bigg\{ &(1 + \langle F' \rangle)^2 P_{\mathrm{L}}(k) + \frac{9}{98}Q_1(k) + \frac{3}{7}Q_2(k) + \frac{1}{2}Q_3(k) \\
&+ \langle F' \rangle\left[\frac{6}{7}Q_5(k) + 2Q_7(k)\right] + \langle F'' \rangle\left[\frac{3}{7}Q_8(k) + Q_9(k)\right] \\
&+ \langle F' \rangle^2 \left[Q_9(k) + Q_{11}(k)\right] + 2\langle F' \rangle\langle F'' \rangle Q_{12}(k) \\
&+ \frac{1}{2}\langle F'' \rangle^2 Q_{13}(k) + \frac{6}{7}\left(1 + \langle F' \rangle\right)^2 \left[R_1(k) + R_2(k)\right] \\
&- \frac{8}{21}\left(1 + \langle F' \rangle\right)R_1(k)\Bigg\},
\end{aligned}
\tag{34}
$$

where

$$k_{\mathrm{NL}} = \left[\frac{1}{6\pi^2}\int dk P_{\mathrm{L}}(k)\right]^{-1/2}, \tag{35}$$

and the functions $Q_n(k)$, $R_n(k)$ are given by Eqs. (A39)–(A48), and are second order in $P_{\mathrm{L}}(k)$. When the exponential prefactor is expanded and only second order terms in $P_{\mathrm{L}}(k)$ are retained, we obtain an expression of EPT without any resummation of higher-order perturbations. In an unbiased case, $\langle F' \rangle = \langle F'' \rangle = 0$, the expression reduces to the result of the one-loop perturbation theory of mass [24, 48].

The power spectrum of the biased objects in redshift space with one-loop corrections is given in Eq. (A69):

$$
\begin{aligned}
P_{\mathrm{obj}}^{(\mathrm{s})}(\boldsymbol{k}) = \exp&\left\{-\left[1 + f(f+2)\mu^2\right](k/k_{\mathrm{NL}})^2\right\} \\
\times &\left[\left(1 + \langle F' \rangle + f\mu^2\right)^2 P_{\mathrm{L}}(k) + \sum_{n,m}\mu^{2n}f^m E_{nm}(k)\right], \tag{36}
\end{aligned}
$$

where $E_{nm}(k)$ is given by Eqs. (A71)–(A79). When the bias is not present, $\langle F' \rangle = \langle F'' \rangle = 0$, this result reduces to the one derived in paper I [48].

A cross power spectrum of differently biased objects is similarly given. When the bias functions of these objects are F_1 and F_2, the cross power spectrum is given by substitutions of Eqs. (A18)–(A22), after expanding Eq. (34) or (36) in terms of $\langle F' \rangle$ and $\langle F'' \rangle$. The spherical average of Eq. (36) can be obtained by using the following integral:

$$
\begin{aligned}
\frac{1}{2}\int_{-1}^{1}d\mu e^{-x\mu^2}\mu^{2n} &= \frac{1}{2}x^{-n-1/2}\gamma\left(n + \frac{1}{2}, x\right) \\
&= (-1)^n \frac{\sqrt{\pi}}{2}\left(\frac{d}{dx}\right)^n\left[\frac{\mathrm{erf}(x^{1/2})}{x^{1/2}}\right], \tag{37}
\end{aligned}
$$

where $\gamma(a, x)$ is the lower incomplete gamma function, and erf is the error function normalized by $\mathrm{erf}(+\infty) = 1$. The correlation function is obtained by numerically Fourier transforming Eq. (36). Spherically averaged correlation function is simply given by

$$\xi(r) = \int_0^\infty \frac{k^2 dk}{2\pi^2}j_0(kr)P(k), \tag{38}$$

where $P(k)$ is the spherically averaged power spectrum.

As described in paper I, the origin of the exponential prefactor $\exp[-(k/k_{\mathrm{NL}})^2]$ is the nonlinear smearing effect by random motions of mass elements. In redshift space, additional smearing effect is present along the lines of sight. The latter effect is similar to the nonlinear fingers-of-God effect [17]. The form of exponential prefactor coincides with the one which has been phenomenologically introduced in previous work [12, 21] to represent the smearing effects.

The one-loop corrections in Eqs. (34) and (36) are given by k-dependent functions, $Q_1(k), \ldots, Q_{13}(k), R_1(k), R_2(k)$, which are defined by Eqs. (A39)–(A48) in the Appendix. All of these functions but $Q_{13}(k)$ vanish in a large-scale limit $k \to 0$. The function $Q_{13}(k)$ contributes only when $\langle F'' \rangle \neq 0$. Thus, the one-loop contributions are present even in a large-scale limit through $Q_{13}(k)$ when $\langle F'' \rangle \neq 0$. This function turns out to be a convolution of the power spectrum,

$$Q_{13}(k) = \int \frac{d^3p}{(2\pi)^3}P_{\mathrm{L}}(p)P_{\mathrm{L}}(|\boldsymbol{k} - \boldsymbol{p}|) = \int d^3x\, e^{-i\boldsymbol{k}\cdot\boldsymbol{x}}\left[\xi_{\mathrm{L}}(x)\right]^2, \tag{39}$$

where $\xi_{\mathrm{L}}(x)$ is the linear correlation function in real space. In configuration space, $[\xi_{\mathrm{L}}(x)]^2 \ll \xi_{\mathrm{L}}(x)$ in a large-scale limit, $x \to \infty$. However, in Fourier space, $Q_{13}(k)$ has a finite value in a large-scale limit,

$$Q_{13}(k \to 0) = \int \frac{d^3p}{(2\pi)^3}\left[P_{\mathrm{L}}(p)\right]^2 = \int d^3x\left[\xi_{\mathrm{L}}(x)\right]^2, \tag{40}$$

while $P_L(k \to 0) = 0$ for cold dark matter (CDM)-like power spectra. Therefore, the power spectrum on very large scales is dominated by a constant contribution originated from non-linear clustering when the bias is present and $\langle F'' \rangle \neq 0$. For related discussion within a framework of local Eulerian bias, see Ref. [20].

E. Nonequivalence between the local Lagrangian bias and the local Eulerian bias

In our local Lagrangian biasing scheme, bias parameters are given by a set of parameters, $\{\langle F^{(n)} \rangle\}$. In the local Eulerian biasing scheme, on the other hand, bias parameters are given by a set of parameters $\{b_n\}$ which are coefficients of a Taylor expansion,

$$\delta_{\mathrm{obj}} = \sum_{n=0}^{\infty} \frac{b_n}{n!} \delta^n, \tag{41}$$

where δ_{obj} is the overdensity of objects and δ is the evolved overdensity of mass at the same Eulerian position with some smoothing filter. One may wonder if there are some relations between these two sets of bias parameters. However, the two biasing schemes are not equivalent to each other, and the two sets of bias parameters are not expressible from one another in general. Therefore, the expression of the biased power spectrum derived above is essentially different from the one with local Eulerian bias previously derived in literature. Below we clarify this situation in detail.

An essential difference between those two schemes is that the Eulerian bias is applied to dynamically evolved density fields while the Lagrangian bias is applied to initial density fields. Since the dynamical evolution is generally nonlocal, those two local biasing schemes are not equivalent to each other.

In the standard halo approach, however, the Eulerian bias parameters $\{b_n\}$ are derived [34, 41], although the halo bias falls into a category of local Lagrangian bias. One may wonder if the local Lagrangian bias is actually equivalent to the local Eulerian bias from this fact. However, the spherical collapse model is crucially assumed in such a derivation. Since the dynamical evolution in a spherical collapse model is locally determined, the local Lagrangian bias and the local Eulerian bias have one-to-one correspondence in such a special case. It is only when the dynamical evolutions are treated approximately as local processes that both biasing schemes become equivalent to each other.

Similarly, the linear dynamical evolution is locally determined, and there is a relation between linear bias parameters of two schemes, $b_1 = 1 + \langle F' \rangle$. This is the reason why the linear power spectrum of Eq. (29) or (32) is equivalent to that with Eulerian linear bias. There are not such relations for higher-order bias parameters in general.

Accordingly, our one-loop result cannot be obtained by just a reparametrization or renormalization of a set of parameters $\{b_n\}$ in one-loop EPT with local Eulerian bias. The power spectrum with local Eulerian bias has a strong dependence on an artificial smoothing length, and has a divergent result in a limit of small smoothing length for CDM-like power spectra [27, 30]. The power spectrum with local Lagrangian bias derived above does not have such a strong dependence and one can safely take the limit. Therefore the two power spectra have qualitatively different properties and are never equivalent to each other. The strong dependence on smoothing length with local Eulerian bias can be removed by a renormalization scheme of McDonald [29]. Even in this case, the resulting power spectrum [Eq. (16) of Ref. [29]] is not reachable by simple reparameterizations of our Eq. (34), and vice versa. For example, McDonald's Eq. (16) has a common factor of b_1^2, while the factor $(1 + \langle F' \rangle)^2$ cannot be factorized out in our Eq. (34) with any reparameterization of $\langle F'' \rangle$.

III. THE HALO BIAS IN PERTURBATION THEORY

A. The halo approach as a local Lagrangian biasing scheme

The nonlinear power spectrum derived above depends on the local Lagrangian bias only through $\langle F^{(n)} \rangle$ defined by Eq. (25). Up to one-loop corrections, we only need two numbers, $\langle F' \rangle$ and $\langle F'' \rangle$. For a general local Lagrangian bias, these numbers could be considered as parameters which should be fitted by observations. Alternatively, those numbers can be derived once a model of bias function $F(\delta)$ is specified. In this section, we take the latter approach, considering the halo bias model.

So far the most successful biasing model in nonlinear structure formation is provided by the halo approach [33, 34, 35, 36, 37, 38, 39, 40, 41], which is based on the extended PS theory [42, 43]. In the PS formalism, the mass of halo is related to the Lagrangian radius R of spherical cell by $M = 4\pi\bar{\rho}R^3/3$, or $R = [M/(1.162 \times 10^{12} h^{-1} M_\odot \Omega_m)]^{1/3} h^{-1}$Mpc, where $M_\odot = 1.989 \times 10^{30}$ kg is the solar mass, and Ω_m is the density parameter at the present time. The variance of mass overdensity in the cell, as a function of mass scale, which is linearly extrapolated to the present time $z = 0$, is given by

$$\sigma^2(M) = \int \frac{k^2 dk}{2\pi^2} W^2(kR) P_0(k), \tag{42}$$

where $W(x) = 3(\sin x - x \cos x)/x^3$ is the top-hat window function, $P_0(k) = P_L(k)/D^2$ is the linear power spectrum extrapolated to the present time.

The critical overdensity, which is required for spherical collapse at redshift z, and is linearly extrapolated to the present time, is given by

$$\delta_c(z) = \frac{\delta_c(0)}{D(z)} \tag{43}$$

where $D(z)$ is the linear growth rate as a function of redshift z, normalized as $D(0) = 1$. The critical overdensity at the present time, $\delta_c(0)$, is given by $\delta_c(0) = 3(3\pi/2)^{2/3}/5 = 1.68647$ in the Einstein-de Sitter model. In general cosmology, δ_c depends weakly on cosmological parameters and redshift [56]. It is still a good approximation to use the constant

value of the Einstein-de Sitter universe in general cosmological models.

According to the PS theory, the comoving number density of haloes with mass between M and $M + dM$, identified at redshift z, is given by

$$n(M, z)dM = \frac{2\bar{\rho}}{M}g(\nu)\frac{d\nu}{\nu}, \qquad (44)$$

where $\nu = \delta_c(z)/\sigma(M)$, $g(\nu) = (2\pi)^{-1/2}\nu\exp(-\nu^2/2)$, and $\bar{\rho}$ is the comoving mean density of mass. In literature, a multiplicity function $f(\tilde{\nu})$ defined by $g(\nu) = \tilde{\nu}f(\tilde{\nu})/2$ and $\tilde{\nu} = \nu^2$ is frequently introduced. The PS mass function is improved by Sheth and Tormen (ST) [36] to give a better fit to that of haloes in numerical simulations of CDM-type cosmologies. The ST mass function is also given by Eq. (44) with a modified function

$$g(\nu) = \frac{A(p)}{\sqrt{2\pi}}\left[1 + \frac{1}{(q\nu^2)^p}\right]\sqrt{q}\,\nu e^{-q\nu^2/2}, \qquad (45)$$

where $A(p) = [1 + \pi^{-1/2}2^{-p}\Gamma(1/2 - p)]^{-1}$, and $p = 0.3$ and $q = 0.707$ are numerically fitted parameters. The PS mass function is also given by Eq. (45) with $p = 0$ and $q = 1$. The Eq. (45) has the following normalization,

$$\int_0^\infty g(\nu)\frac{d\nu}{\nu} = \frac{1}{2}, \qquad (46)$$

which is equivalent to $\int n(M, z)MdM = \bar{\rho}$.

The original PS theory is extended to give the number density of haloes of mass M_1, identified at redshift z_1, in a region of Lagrangian radius R_0 in which the linear overdensity extrapolated to the present time is δ_0:

$$n(M_1, z_1|\delta_0, R_0)dM_1 = \frac{2\bar{\rho}}{M_1}g(\nu_{10})\frac{d\nu_{10}}{\nu_{10}}, \qquad (47)$$

where

$$\nu_{10} = \frac{\delta_1 - \delta_0}{\left(\sigma_1^2 - \sigma_0^2\right)^{1/2}}, \qquad (48)$$

$$\delta_1 = \delta_c(z_1), \quad \sigma_0 = \sigma(M_0), \quad \sigma_1 = \sigma(M_1) \qquad (49)$$

and $M_0 = 4\pi\bar{\rho}R_0^3/3$. The haloes of mass M_1 are collapsed at z_1, while M_0 is assumed uncollapsed at $z = 0$, and thus we always have $\delta_1 > \delta_0$.

The conditional number density of Eq. (47) is interpreted as a large-scale spatial modulation of halo densities in Lagrangian space. The number density of haloes is a function of the linearly extrapolated overdensity with smoothing radius R_0. Therefore, Eq. (47) corresponds to the Lagrangian number density of biased objects in Eq. (6) for haloes of mass between M_1 and $M_1 + dM_1$. The bias function for the halo bias is given by

$$F_{M_1}(\delta_0) = \frac{n(M_1, z_1|\delta_0, R_0)dM_1}{n(M_1, z_1)dM_1}, \qquad (50)$$

where the mass scale M_1 is explicitly denoted. Defining $\nu_1 = \delta_1/\sigma_1$, we have

$$\frac{d\nu_{10}/\nu_{10}}{d\nu_1/\nu_1} = \frac{\sigma_1^2}{\sigma_1^2 - \sigma_0^2}, \qquad (51)$$

where $\nu_1, \nu_{10}, \sigma_1, \sigma_0$ are considered as functions of halo mass M_1. Combining Eqs. (44), (47), (50), and (51), the halo bias function reduces to

$$F_{M_1}(\delta_0) = \frac{\sigma_1^2}{\sigma_1^2 - \sigma_0^2}\frac{g(\nu_{10})}{g(\nu_1)}. \qquad (52)$$

Since the RHS of Eq. (52) depends on δ_0 only through $\delta_1 - \delta_0$ of ν_{10}, we have

$$\left\langle\left(\frac{\partial}{\partial\delta_0}\right)^n g(\nu_{10})\right\rangle = \left(-\frac{\partial}{\partial\delta_1}\right)^n\langle g(\nu_{10})\rangle, \qquad (53)$$

where the average $\langle\cdots\rangle$ is taken over distribution of δ_0. Assuming the initial density field is Gaussian, the distribution of δ_0 is also Gaussian with variance σ_0^2. In the case of PS mass function, $p = 0$ and $q = 1$, a Gaussian integral to give the average $\langle g(\nu_{10})\rangle$ can be exactly performed:

$$\langle g(\nu_{10})\rangle = \frac{1}{\sqrt{2\pi\sigma_0^2}}\int_{-\infty}^\infty d\delta_0\,e^{-\delta_0^2/2\sigma_0^2}g(\nu_{10})$$

$$= \frac{\sigma_1^2 - \sigma_0^2}{\sigma_1^2}g(\nu_1). \qquad (54)$$

In a general case of ST mass function, $p \neq 0$ and $q \neq 1$, Eq. (54) is shown in a limit $\sigma_0 \ll \sigma_1$, which is a reasonable approximation when M_0 is much larger than M_1.

From Eqs. (52)–(54), we have

$$\left\langle F_{M_1}^{(n)}\right\rangle = \frac{(-1)^n}{g(\nu_1)}\left(\frac{\partial}{\partial\delta_1}\right)^n g(\nu_1) = \frac{(-1)^n\nu_1^n}{\delta_1^n\,g(\nu_1)}\frac{\partial^n g(\nu_1)}{\partial\nu_1^n}. \qquad (55)$$

With this expression, the following consistency relation is straightforwardly shown:

$$\frac{1}{\bar{\rho}}\int_0^\infty dM_1 n(M_1, z_1)M_1\left\langle F_{M_1}^{(n)}\right\rangle = \begin{cases}1, & n = 0, \\ 0, & n \geq 1.\end{cases} \qquad (56)$$

For our purpose of one-loop corrections, we need only first two derivatives. Dropping the subscript M and '1', they are given by

$$\langle F'\rangle = \frac{1}{\delta_c(z)}\left[q\nu^2 - 1 + \frac{2p}{1 + (q\nu^2)^p}\right], \qquad (57)$$

$$\langle F''\rangle = \frac{1}{\delta_c{}^2(z)}\left[q^2\nu^4 - 3q\nu^2 + \frac{2p\left(2q\nu^2 + 2p - 1\right)}{1 + (q\nu^2)^p}\right], \qquad (58)$$

where $\nu = \delta_c(z)/\sigma(M)$. The Eulerian bias factor of Eq. (31) with Eq. (57) agrees with that of the original halo approach [33, 34, 36]. In Fig. 1, $\langle F'\rangle$ and $\langle F''\rangle$ are plotted against mass of haloes. We adopt cosmological parameters $\Omega_m = 0.28$,
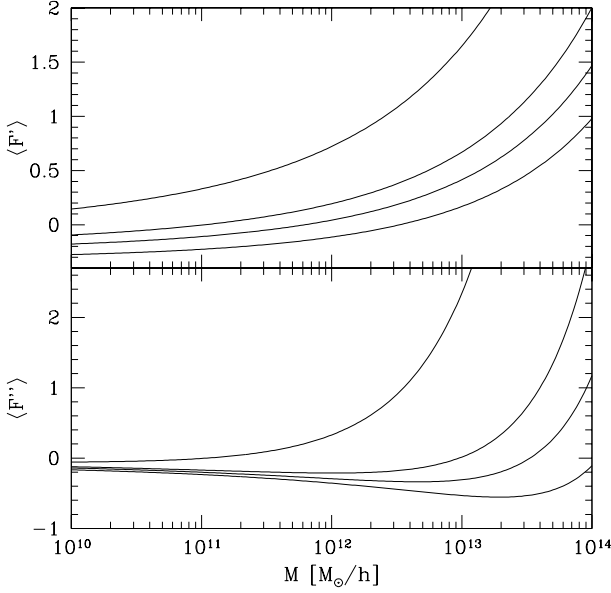
FIG. 1: Local Lagrangian bias parameters $\langle F' \rangle$, $\langle F'' \rangle$ as functions of halo mass. Different curves correspond to different redshifts ($z = 0, 0.5, 1, 3$ from bottom to top in each panel).

$\Omega_\Lambda = 0.72$, $\Omega_b = 0.046$, $h = 0.7$, $n_s = 0.96$ and $\sigma_8 = 0.82$ and the linear power spectrum $P_0(k)$ is calculated from the output of the CAMB code [57]. This set of parameters is always assumed in the following figures throughout this paper.

When a finite range of mass $[M_1, M_2]$ of haloes is considered, the denominator and the numerator of Eq. (50) are altered into integrations in that range. The above derivation is similarly applied in this case. As a result, we have

$$\left\langle F^{(n)} \right\rangle = \frac{(-1)^n}{\delta_c^{\,n}(z)} \frac{\displaystyle\int_{M_1}^{M_2} \nu^n \frac{d^n g}{d\nu^n} \frac{d\ln\sigma}{dM} \frac{dM}{M}}{\displaystyle\int_{M_1}^{M_2} g(\nu) \frac{d\ln\sigma}{dM} \frac{dM}{M}}. \tag{59}$$

In a limit $M_2 \to M_1$, the Eq. (55) is recovered as expected.

B. Scale-dependence of the bias in quasi-linear regime

Applying Eqs. (57) and (58) to our results of Eq. (34) or Eq. (36), a power spectrum of haloes with one-loop corrections, either in real space or in redshift space, can be evaluated. To demonstrate the effects of biasing and redshift-space distortions, we show examples of power spectra and correlation functions in this subsection, and briefly discuss the impact on BAO features. Since the main purpose of the present paper is to give a new formalism in perturbation theory, detailed investigation of BAOs with our approach will be given elsewhere.

In Fig. 2, the normalized power spectra in real space are plotted, and those in redshift space are shown in Fig. 3. We adopt the same set of cosmological parameters as in Fig. 1. Angular averages are taken for power spectra in redshift

space. In paper I, it is shown that our one-loop formula is valid within a few percent for $k < k_{NL}/2$ [48], compared to numerical simulations. Expecting this criterion is also effective in our generalization including bias, the corresponding scales of validity, $k_{NL}/2$, are shown in vertical dotted lines in the figures. To highlight nonlinear effects, overall amplitudes predicted from linear growth rate, linear bias and linear redshift-space distortions are scaled out. In real space, the amplitude of power spectrum is proportional to a scale-independent factor $D^2(z)b^2(z)$, where $b(z)$ is the linear bias factor defined by Eq. (31). In redshift space, Kaiser's enhancement factor $R(z) = 1 + 2\beta/3 + \beta^2/5$ [18] is an additional source of the linear amplitude.

In upper panels in the figures, each power spectrum is normalized by a smoothed, no-wiggle linear power spectrum $P_{nw}(k)$ of Ref. [58] to highlight baryonic features. The linear amplification factors described above are all scaled out. In lower panels, power spectra of haloes divided by those of dark matter are plotted, where amplifications by linear biases and linear redshift-space distortions are scaled out. Thus, curves in lower panels show the scale dependence of bias. In the usual halo approach, the scale dependence of the bias arises only from galaxy/dark matter clustering within haloes, which is not considered in this paper. The scale dependence shown in our results purely originates in clustering of haloes themselves. Linear theory predicts constancy of halo bias on large scales. Nonlinear effects of dynamics, biasing, and redshift-space distortions are responsible for the scale dependence.

Comparing the clustering in real space and in redshift space, the power spectra on small scales are suppressed by nonlinear redshift-space distortions. This suppression is due to the large-scale random motion of objects, which is similar to a phenomenon known as a fingers-of-God effect [17] on small scales. Generally, the scale dependence of bias is strong for very massive and very light haloes. Haloes of intermediate mass do not show significant deviations from constant bias. The scale dependence of bias does not show significant oscillations, and are mostly smooth functions of scales. This is desirable for cosmological applications to use the BAO scale as a standard ruler. Various nonlinear effects mostly modify the broadband shape of power spectrum, and therefore resulting shifts of acoustic scales are correctable as numerically demonstrated in Ref. [59].

Although the power spectrum and correlation function are related by Fourier transforms and have mathematically equivalent information, cosmological information that can be extracted from them with real data is not exactly equivalent to each other, because error properties are different. While the BAO scales are imprinted in multiple wiggles in the power spectrum, there appears one single peak in the correlation function [8]. The physical BAO scale is just a single scale, and many wiggles in the power spectrum are overtones of the fundamental scale of BAOs. In Figs. 4 and 5, correlation functions are plotted. They are calculated by Fourier transforming the power spectra of Figs. 2 and 3. In paper I, we have shown that our method of one-loop corrections to the clustering of dark matter, both in real space and in redshift space, agrees very well with numerical simulations on scales
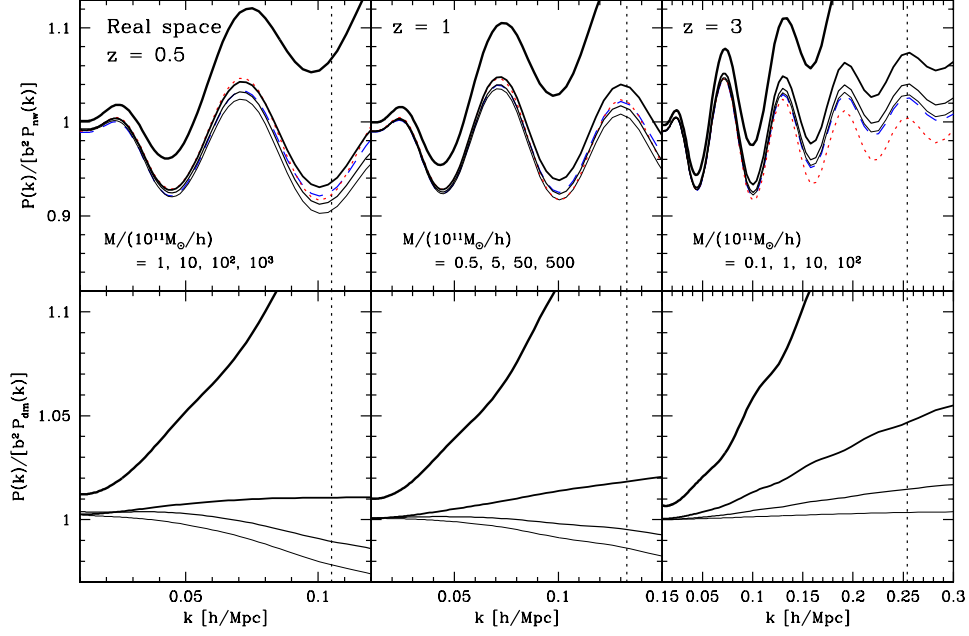
FIG. 2: Dependencies on halo mass and redshift of nonlinear power spectrum in real space. In the top panels, each power spectrum is divided by a smoothed, no-wiggle linear power spectrum $P_{\mathrm{nw}}(k)$ [58], and by a squared linear bias factor b^2. Values of redshifts and halo masses are shown in each panel. Solid lines: nonlinear power spectra of haloes with different masses with increasing order from thinner to thicker lines; dotted lines: linear theory; dashed lines: nonlinear power spectra of dark matter. In the bottom panels, halo power spectra are divided by corresponding mass power spectra and by squared linear bias factor, presenting the scale dependence of halo bias. Vertical short-dashed lines correspond to the scale $k_{\mathrm{NL}}/2$ to indicate the validity range $k < k_{\mathrm{NL}}/2$, where our result is expected to be accurate within a few percent.
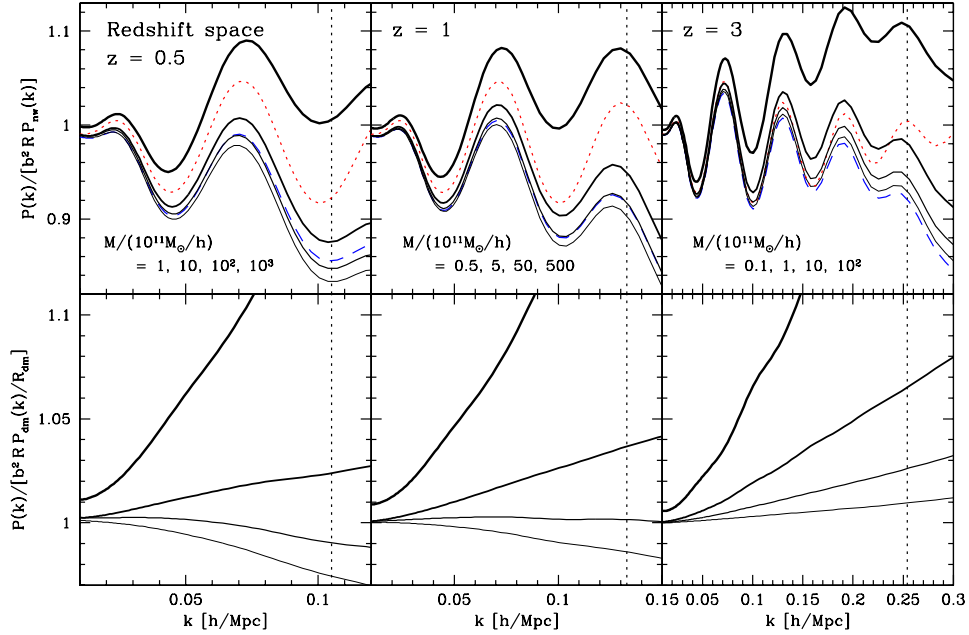

FIG. 3: Same as Fig. 2, but in redshift space. Spherically averaged power spectra are plotted. Linear redshift-space enhancement factor $R = 1 + 2\beta/3 + \beta^2/5$ is also scaled out.
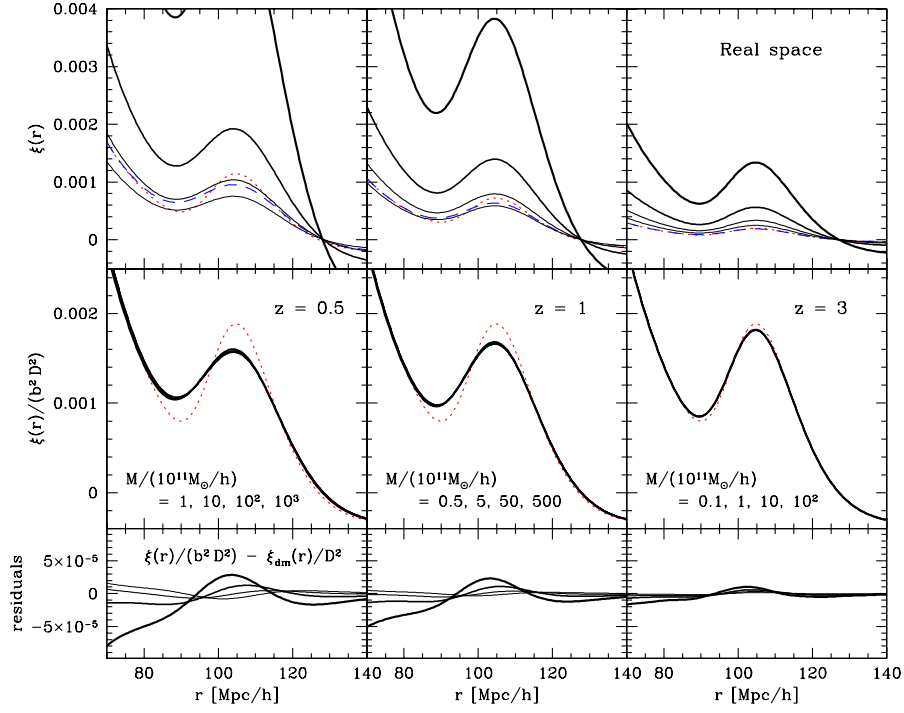
FIG. 4: Dependencies on halo mass and redshift of nonlinear correlation function in real space. Correlation functions with a fixed redshift and with different halo masses are presented in each column. Mass of the halo varies in increasing order from thinner to thicker solid lines. Dotted lines correspond to the prediction of linear theory and dashed lines correspond to nonlinear correlation functions of dark matter. In the top rows, the bare values of correlation function are plotted. In the middle rows, the correlation functions are normalized by linear bias factors and linear growth factors. In the bottom rows, residual values in the normalized correlation function of haloes (plotted in middle rows), relative to that of dark matter, are plotted.
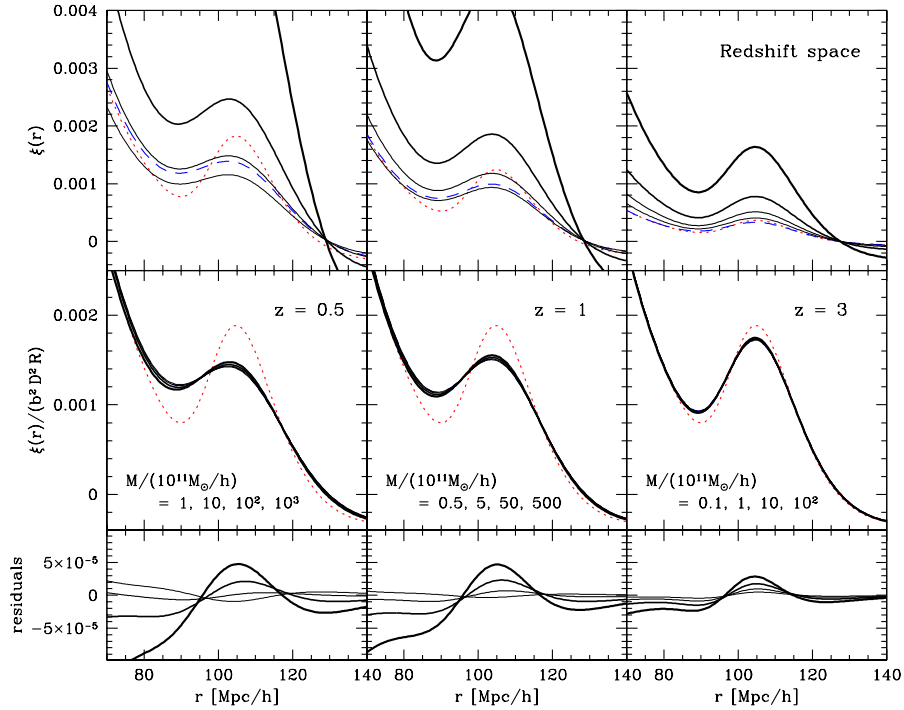

FIG. 5: Same as Fig. 4, but in redshift space. Spherically averaged correlation functions are plotted. Linear redshift-space enhancement factor R is also scaled out.

$r > 70\,h^{-1}\mathrm{Mpc}$, where BAO signatures appear. Upper panels show bare correlation functions, and middle panels show normalized correlation functions. The overall amplitudes of the linear growth rate, linear bias and linear redshift-space distortions are scaled out in the normalized plots. The normalized correlation functions do not significantly depend on mass of haloes, and plotted lines are quite overlapped. In lower panels, residual values relative to normalized correlation functions of dark matter are plotted.

Nonlinear effects degrade the signature of the BAO peak because of random displacements of haloes, and the degradation is larger in redshift space because of additional displacements along the lines of sight. Halo bias does not significantly change the shape of the BAO peak. This property is consistent with a recent analysis of numerical simulations of halo clustering [14]. Effects of nonlinear dynamics and nonlinear redshift-space distortions dominate those of nonlinear halo bias. Massive haloes slightly enhance the BAO signature by 5% or so, while less massive haloes only change by 1–2%. The effects are slightly larger in redshift space.

IV. SUMMARY

In this paper, we show that the nonlinear perturbation theory via the Lagrangian picture is naturally incorporated with the local Lagrangian bias on top of the redshift-space distortions. Explicit results of one-loop power spectrum with a halo bias both in real space and in redshift space are given. Our approach does not suffer from a conceptual problem which appears in the EPT with local Eulerian bias. The halo bias, as a local Lagrangian bias, is properly treated in the Lagrangian picture of perturbations. Simultaneous inclusion of redshift-space distortions is also natural in the Lagrangian picture. Our approach involves a partial resummation of Eulerian perturbations, and provides a better description in the quasilinear regime than the standard EPT.

In our general framework of local Lagrangian bias, the bias is characterized by local Lagrangian bias parameters $\langle F^{(n)} \rangle$. We do not need a Taylor expansion of the bias function as frequently adopted in local Eulerian biasing scheme. Only the first two of the local Lagrangian bias parameters are needed in our one-loop calculations. The results in Sec. II are applicable for all biasing schemes as long as the bias is local in Lagrangian space. The local Lagrangian bias parameters are considered as free parameters if the bias model is not specified. Because of the nonlocal nature of gravitational evolution, the local Lagrangian biasing scheme is not equivalent to the local Eulerian biasing scheme.

There is a successful model of Lagrangian bias, i.e., the halo bias. The general halo approach consists of several pieces of assumptions. We adopt only the most fundamental concept of the halo approach, the halo bias in Lagrangian space. The clustering of galaxies or dark matter is dominated by halo clustering on large scales, where the perturbation theory is safely applied. As a result, the local Lagrangian bias parameters are calculated for halo bias without ambiguity. The resulting power spectrum does not have any free parameters once

the mass or mass range of haloes is specified.

In usual linear analysis, the halo bias is independent on scales. However, nonlinear effects introduce the scale dependence into the halo bias. Such scale dependence could affect the determination of the BAO scales unless the effect is properly quantified. Such effects are quantitatively calculated without numerical simulations. We find that the scale dependence of bias is a smoothly varying function. Therefore, the BAO scales are shifted by change of the broadband shape in the power spectrum. The correlation function is also affected by scale dependence of nonlinear halo bias. Compared to the power spectrum, the shape of the BAO peak in the correlation function seems to be less affected. Those observations are consistent with the recent results of numerical simulations [13, 14].

Our formalism is compatible with any biasing scheme which is local in Lagrangian space. For example, the peak bias is approximately considered as a local in Lagrangian space in a limit of the peak-background split [16, 34], when the constraints imposed by the spatial derivatives to define peaks can be neglected. However, the last approximation may not be appropriate for accurately predicting the BAO signature [60]. The exact biasing mechanism in the real world is definitely not local both in Eulerian space and in Lagrangian space. The success of the halo approach indicates the local Lagrangian bias is a good approximation at least on large scales. However, extending the model of local Lagrangian bias to a nonlocal one is an option to make the theory more accurate and general. It is straightforward to extend our formalism in Sec. II to include a nonlocal bias.

Although our formalism contains a partial resummation of higher-order Eulerian perturbations, Lagrangian perturbations are truncated at the one-loop level. Recent developments of the renormalized perturbation theory and its variants [49] show that it is possible to reorganize and resum higher-order perturbations using the concept of propagators. It would be interesting if one could use the concept of propagators in Lagrangian space [61] to further renormalize the present formalism and to describe the deeply nonlinear regime, $k > k_{\mathrm{NL}}/2$, which is not accessible by the present formalism.

We consider only the halo bias in this paper. The resulting power spectrum corresponds to that of halo centers, or the two-halo term of the halo model on large scales. In the halo approach, the nonlinear power spectrum is given by a superposition of the one-halo term and the two-halo term, which are given by convolutions with a model of density profile of galaxies or dark matter. A model of density profile is dominantly relevant to clustering on small scales. In a context of the halo approach, our formalism improves the description of the two-halo term, in which only the linear dynamics is usually included because of simplicity. It is possible to include a model of density profile of halo model in redshift space [62].

As pointed out in paper I, our approach does not have much power on small scales in the power spectrum, $k > k_{\mathrm{NL}}/2$. The main source of the powerless is the exponential damping factor, which originates from random motion of the displacement field. A fully nonlinear description of this factor may dramatically improve the applicability of the present formalism

for dark matter clustering. However, in the presence of bias, the nonlinear regime is dominated by the scale dependence of bias, which may be more appropriately described by halo approach with the one-halo term, including a model of density profile or halo occupation dynamics.

APPENDIX A: ONE-LOOP CORRECTIONS TO THE BIASED POWER SPECTRUM VIA THE LAGRANGIAN PERTURBATION THEORY

In this Appendix, we outline a derivation of one-loop corrections to the power spectrum with the local Lagrangian bias. Our goal is to evaluate the cumulants of Eq. (14) by the perturbation theory, and obtain a perturbative expansion of Eq. (24). Most of the necessary techniques have been developed in paper I [48].

For the one-loop corrections, the cumulants of Eq. (14) up to second order in $P_L(k)$ should be evaluated. We have applied the LPT [46, 48] to evaluate the similar cumulants in paper I, and we can use the same method. In the LPT, the displacement field $\boldsymbol{\Psi}$ is expanded by a perturbative series:

$$\boldsymbol{\Psi} = \boldsymbol{\Psi}^{(1)} + \boldsymbol{\Psi}^{(2)} + \boldsymbol{\Psi}^{(3)} + \cdots . \tag{A1}$$

The first-order term $\boldsymbol{\Psi}^{(1)}$ corresponds to the classic Zel'dovich approximation [63]. The spatial derivatives of each term, $\partial_i \Psi_j^{(n)}$ have the order of $O(\delta_L)^n$, where δ_L is the linear density field. In a Fourier representation,

$$\tilde{\boldsymbol{\Psi}}^{(n)}(\boldsymbol{p}) = \frac{i}{n!} \int \frac{d^3 p_1}{(2\pi)^3} \cdots \frac{d^3 p_n}{(2\pi)^3} (2\pi)^3 \delta_D^3 \left(\sum_{j=1}^n \boldsymbol{p}_j - \boldsymbol{p} \right)$$
$$\times \boldsymbol{L}^{(n)}(\boldsymbol{p}_1, \ldots, \boldsymbol{p}_n) \delta_L(\boldsymbol{p}_1) \cdots \delta_L(\boldsymbol{p}_n), \quad \text{(A2)}$$

where $\delta_L(\boldsymbol{p})$ is the Fourier transform of the linear density field, and perturbative kernels $\boldsymbol{L}^{(n)}$ are given by the LPT. Since the dependence of these kernels on time and on cosmological parameters is weak, it is a good approximation to use the kernels of the Einstein-de Sitter model even in general cosmology [54]. In real space, expressions of the kernels $\boldsymbol{L}^{(n)}$ up to

third order are given by [48, 64]

$$\boldsymbol{L}^{(1)}(\boldsymbol{p}_1) = \frac{\boldsymbol{k}}{k^2}, \tag{A3}$$

$$\boldsymbol{L}^{(2)}(\boldsymbol{p}_1, \boldsymbol{p}_2) = \frac{3}{7} \frac{\boldsymbol{k}}{k^2} \left(1 - \mu_{1,2}^2 \right), \tag{A4}$$

$$\boldsymbol{L}^{(3a)}(\boldsymbol{p}_1, \boldsymbol{p}_2, \boldsymbol{p}_3) = \frac{5}{7} \frac{\boldsymbol{k}}{k^2} \left(1 - \mu_{1,2}^2 \right)\left(1 - \mu_{12,3}^2 \right)$$
$$- \frac{1}{3} \frac{\boldsymbol{k}}{k^2} \left(1 - 3\mu_{1,2}^2 + 2\mu_{1,2}\mu_{2,3}\mu_{3,1} \right) + \boldsymbol{k} \times \boldsymbol{T}(\boldsymbol{p}_1, \boldsymbol{p}_2, \boldsymbol{p}_3), \tag{A5}$$

where $\boldsymbol{k} = \boldsymbol{p}_1 + \cdots + \boldsymbol{p}_n$ for each $\boldsymbol{L}^{(n)}$, $\mu_{i,j} = \boldsymbol{p}_i \cdot \boldsymbol{p}_j/(p_i p_j)$, $\mu_{ij,k} = (\boldsymbol{p}_i + \boldsymbol{p}_j) \cdot \boldsymbol{p}_k/(|\boldsymbol{p}_i + \boldsymbol{p}_j|p_k)$, and a vector $\boldsymbol{T}$ represents a transverse part whose expression is not needed in the following application. It is useful to symmetrize the kernel $\boldsymbol{L}^{(3a)}$ in terms of their arguments:

$$\boldsymbol{L}^{(3)}(\boldsymbol{p}_1, \boldsymbol{p}_2, \boldsymbol{p}_3) = \frac{1}{3} \left[\boldsymbol{L}^{(3a)}(\boldsymbol{p}_1, \boldsymbol{p}_2, \boldsymbol{p}_3) + \text{perm.} \right]. \tag{A6}$$

As shown in paper I, the perturbative kernels in redshift space are simply given by linear transformations by redshift-space distortion tensors $R^{(n)}$, whose components are

$$R_{ij}^{(n)} = \delta_{ij} + n f \hat{z}_i \hat{z}_j, \tag{A7}$$

where $f = d \ln D/d \ln a = (HD)^{-1}\dot{D}$ is the logarithmic derivative of linear growth rate $D(t)$ by the scale factor $a(t)$, and $\hat{z}_i$ is a unit vector along the line of sight. In a matrix notation, the kernels in redshift space is given by

$$\boldsymbol{L}^{s(n)} = R^{(n)} \boldsymbol{L}^{(n)}. \tag{A8}$$

It is useful to define the following mixed polyspectra of linear density field and displacement field:

$$\left\langle \tilde{\delta}_L(\boldsymbol{k}_1) \cdots \tilde{\delta}_L(\boldsymbol{k}_l) \tilde{\Psi}_{i_1}(\boldsymbol{p}_1) \cdots \tilde{\Psi}_{i_m}(\boldsymbol{p}_m) \right\rangle_c$$
$$= (2\pi)^3 \delta_D^3 (\boldsymbol{k}_1 + \cdots + \boldsymbol{k}_l + \boldsymbol{p}_1 + \cdots + \boldsymbol{p}_m)$$
$$\times (-i)^m C_{i_1 \cdots i_m} (\boldsymbol{k}_1, \ldots, \boldsymbol{k}_l; \boldsymbol{p}_1, \ldots, \boldsymbol{p}_m), \quad \text{(A9)}$$

where $\tilde{\delta}_L$ and $\tilde{\Psi}_i$ are the Fourier transforms of the linear density field and the displacement field, respectively. When $l = 0$, the above polyspectra are equivalent to the ones defined in Eq. (11) of paper I, but we adopt an opposite sign in this paper. For $l + m = 2$ in the Eq. (A9), we also use notations such as

$$C(\boldsymbol{k}) = C(\boldsymbol{k}, -\boldsymbol{k}), \ C_i(\boldsymbol{k}) = C_i(\boldsymbol{k}; -\boldsymbol{k}), \ C_{ij}(\boldsymbol{k}) = C_{ij}(\boldsymbol{k}, -\boldsymbol{k}). \tag{A10}$$

When $m = 0$, the above polyspectra of Eq. (A9) is nonzero only when $l = 2$ for a Gaussian initial condition, which is assumed throughout this paper. The Eq. (14) has the order $O[P_L(k)]^{l_1+l_2+m_1+m_2-1}$, because of the property of cumulants [25]. Therefore, we only need to consider $n_1 + n_2 + m_1 + m_2 \leq 3$ up to one-loop corrections. Expanding the exponential factors in Eq. (24), but the first prefactor, and truncating third-

or higher-order terms in $P_{\mathrm{L}}(k)$, we obtain

$$P_{\mathrm{obj}}(\boldsymbol{k}) = \exp\left[k_i k_j \int \frac{d^3 p}{(2\pi)^3} C_{ij}(\boldsymbol{p}) \right]$$
$$\times \Big[a_{00}(\boldsymbol{k}) + \langle F' \rangle\, a_{10}(\boldsymbol{k}) + \langle F'' \rangle\, a_{01}(\boldsymbol{k}) + \langle F' \rangle^2\, a_{20}(\boldsymbol{k})$$
$$+ \langle F' \rangle \langle F'' \rangle\, a_{11}(\boldsymbol{k}) + \langle F'' \rangle^2\, a_{02}(\boldsymbol{k}) \Big], \quad \text{(A11)}$$

where

$$a_{00}(\boldsymbol{k}) = - k_i k_j C_{ij}(\boldsymbol{k}) - k_i k_j k_k \int \frac{d^3 p}{(2\pi)^3} C_{ijk}(\boldsymbol{k}, -\boldsymbol{p}, \boldsymbol{p} - \boldsymbol{k})$$
$$+ \frac{1}{2} k_i k_j k_k k_l \int \frac{d^3 p}{(2\pi)^3} C_{ij}(\boldsymbol{p}) C_{kl}(\boldsymbol{k} - \boldsymbol{p}), \quad \text{(A12)}$$

$$a_{10}(\boldsymbol{k}) = 2 k_i C_i(\boldsymbol{k})$$
$$+ k_i k_j \int \frac{d^3 p}{(2\pi)^3} \Big[C_{ij}(\boldsymbol{k}; -\boldsymbol{p}, \boldsymbol{p} - \boldsymbol{k}) - 2 C_{ij}(-\boldsymbol{p}; \boldsymbol{p} - \boldsymbol{k}, \boldsymbol{k}) \Big]$$
$$- 2 k_i k_j k_k \int \frac{d^3 p}{(2\pi)^3} C_i(\boldsymbol{p}) C_{jk}(\boldsymbol{k} - \boldsymbol{p}), \quad \text{(A13)}$$

$$a_{01}(\boldsymbol{k}) = - k_i \int \frac{d^3 p}{(2\pi)^3} C_i(-\boldsymbol{p}, \boldsymbol{p} - \boldsymbol{k}; \boldsymbol{k})$$
$$+ k_i k_j \int \frac{d^3 p}{(2\pi)^3} C_i(\boldsymbol{p}) C_j(\boldsymbol{k} - \boldsymbol{p}), \quad \text{(A14)}$$

$$a_{20}(\boldsymbol{k}) = C(\boldsymbol{k}) + 2 k_i \int \frac{d^3 p}{(2\pi)^3} C_i(\boldsymbol{k}, -\boldsymbol{p}; \boldsymbol{p} - \boldsymbol{k})$$
$$+ k_i k_j \int \frac{d^3 p}{(2\pi)^3} \Big[C_i(\boldsymbol{p}) C_j(\boldsymbol{k} - \boldsymbol{p}) - C(\boldsymbol{p}) C_{ij}(\boldsymbol{k} - \boldsymbol{p}) \Big],$$
$$\text{(A15)}$$

$$a_{11}(\boldsymbol{k}) = 2 k_i \int \frac{d^3 p}{(2\pi)^3} C(\boldsymbol{p}) C_i(\boldsymbol{k} - \boldsymbol{p}), \quad \text{(A16)}$$

$$a_{02}(\boldsymbol{k}) = \frac{1}{2} \int \frac{d^3 p}{(2\pi)^3} C(\boldsymbol{p}) C(\boldsymbol{k} - \boldsymbol{p}). \quad \text{(A17)}$$

We have neglected effects of the smoothing kernel $W(kR)$ in the above equation, for the consistency of our treatment as discussed in the end of Sec. III A. A cross power spectrum of differently biased objects is similarly given. When the bias functions of these objects are F_1 and F_2, the cross power spectrum is given by substitutions

$$\langle F' \rangle \to \frac{1}{2} \left(\langle F_1' \rangle + \langle F_2' \rangle \right), \quad \text{(A18)}$$

$$\langle F'' \rangle \to \frac{1}{2} \left(\langle F_1'' \rangle + \langle F_2'' \rangle \right), \quad \text{(A19)}$$

$$\langle F' \rangle^2 \to \langle F_1' \rangle \langle F_2' \rangle, \quad \text{(A20)}$$

$$\langle F'' \rangle^2 \to \langle F_1'' \rangle \langle F_2'' \rangle, \quad \text{(A21)}$$

$$\langle F' \rangle \langle F'' \rangle \to \frac{1}{2} \left(\langle F_1' \rangle \langle F_2'' \rangle + \langle F_1'' \rangle \langle F_2' \rangle \right), \quad \text{(A22)}$$

in Eq. (A11).

Next we define mixed polyspectra of each order in perturbations:

$$\left\langle \tilde{\delta}_{\mathrm{L}}(\boldsymbol{k}_1) \cdots \tilde{\delta}_{\mathrm{L}}(\boldsymbol{k}_l) \tilde{\Psi}_{i_1}^{(n_1)}(\boldsymbol{p}_1) \cdots \tilde{\Psi}_{i_m}^{(n_m)}(\boldsymbol{p}_m) \right\rangle_{\mathrm{c}}$$
$$= (2\pi)^3 \delta_{\mathrm{D}}^3 (\boldsymbol{k}_1 + \cdots + \boldsymbol{k}_l + \boldsymbol{p}_1 + \cdots + \boldsymbol{p}_m)$$
$$\times (-i)^m C_{i_1 \cdots i_m}^{(n_1 \cdots n_m)} (\boldsymbol{k}_1, \ldots, \boldsymbol{k}_l; \boldsymbol{p}_1, \ldots, \boldsymbol{p}_m), \quad \text{(A23)}$$

where $\tilde{\Psi}_i^{(n)}$ are the Fourier transforms of the displacement field of order n in Eq. (A1). For $l + m = 2$ in the Eq. (A23), we also use notations similar to those in Eq. (A10), such as $C^{(n)}(\boldsymbol{k})$, $C_i^{(n)}(\boldsymbol{k})$, $C_{ij}^{(n_1 n_2)}(\boldsymbol{k})$. The Eq. (A23) is nonzero only when $l + n_1 + \cdots + n_m$ is an even number. The original mixed polyspectra of Eq. (A9) are given by sums of the polyspectra of each order. In particular,

$$C_i(\boldsymbol{p}) = C_i^{(1)}(\boldsymbol{p}) + C_i^{(3)}(\boldsymbol{p}) + \cdots, \quad \text{(A24)}$$

$$C_{ij}(\boldsymbol{p}) = C_{ij}^{(11)}(\boldsymbol{p}) + C_{ij}^{(22)}(\boldsymbol{p}) + C_{ij}^{(13)}(\boldsymbol{p}) + C_{ij}^{(31)}(\boldsymbol{p}) + \cdots, \quad \text{(A25)}$$

$$C_i(\boldsymbol{p}_1, \boldsymbol{p}_2; \boldsymbol{p}_3) = C_i^{(2)}(\boldsymbol{p}_1, \boldsymbol{p}_2; \boldsymbol{p}_3) + \cdots, \quad \text{(A26)}$$

$$C_{ij}(\boldsymbol{p}_1; \boldsymbol{p}_2, \boldsymbol{p}_3) = C_{ij}^{(12)}(\boldsymbol{p}_1; \boldsymbol{p}_2, \boldsymbol{p}_3) + C_{ij}^{(21)}(\boldsymbol{p}_1; \boldsymbol{p}_2, \boldsymbol{p}_3) + \cdots, \quad \text{(A27)}$$

$$C_{ijk}(\boldsymbol{p}_1, \boldsymbol{p}_2, \boldsymbol{p}_3) = C_{ijk}^{(112)}(\boldsymbol{p}_1, \boldsymbol{p}_2, \boldsymbol{p}_3)$$
$$+ C_{ijk}^{(121)}(\boldsymbol{p}_1, \boldsymbol{p}_2, \boldsymbol{p}_3) + C_{ijk}^{(211)}(\boldsymbol{p}_1, \boldsymbol{p}_2, \boldsymbol{p}_3) + \cdots, \quad \text{(A28)}$$

up to second order in $P_{\mathrm{L}}(k)$. Using the LPT kernels of Eq. (A2), the mixed polyspectra of each order are given by

$$C(\boldsymbol{p}) = P_{\mathrm{L}}(p), \quad \text{(A29)}$$

$$C_i^{(1)}(\boldsymbol{p}) = L_i^{(1)}(\boldsymbol{p}) P_{\mathrm{L}}(p), \quad \text{(A30)}$$

$$C_{ij}^{(11)}(\boldsymbol{p}) = -L_i^{(1)}(\boldsymbol{p}) L_j^{(1)}(\boldsymbol{p}) P_{\mathrm{L}}(p), \quad \text{(A31)}$$

$$C_i^{(3)}(\boldsymbol{p}) = \frac{1}{2} P_{\mathrm{L}}(p) \int \frac{d^3 p'}{(2\pi)^3} L_i^{(3)}(\boldsymbol{p}, -\boldsymbol{p}', \boldsymbol{p}') P_{\mathrm{L}}(p'), \quad \text{(A32)}$$

$$C_{ij}^{(22)}(\boldsymbol{p}) = -\frac{1}{2} \int \frac{d^3 p'}{(2\pi)^3} L_i^{(2)}(\boldsymbol{p}', \boldsymbol{p} - \boldsymbol{p}') L_j^{(2)}(\boldsymbol{p}', \boldsymbol{p} - \boldsymbol{p}')$$
$$\times P_{\mathrm{L}}(p') P_{\mathrm{L}}(|\boldsymbol{p} - \boldsymbol{p}'|), \quad \text{(A33)}$$

$$C_{ij}^{(13)}(\boldsymbol{p}) = C_{ji}^{(31)}(\boldsymbol{p})$$
$$= -\frac{1}{2} L_i^{(1)}(\boldsymbol{p}) P_{\mathrm{L}}(p) \int \frac{d^3 p'}{(2\pi)^3} L_j^{(3)}(\boldsymbol{p}, -\boldsymbol{p}', \boldsymbol{p}') P_{\mathrm{L}}(p'), \quad \text{(A34)}$$

$$C_i^{(2)}(\boldsymbol{p}_1, \boldsymbol{p}_2; \boldsymbol{p}_3) = L_i^{(2)}(\boldsymbol{p}_1, \boldsymbol{p}_2) P_{\mathrm{L}}(p_1) P_{\mathrm{L}}(p_2), \quad \text{(A35)}$$

$$C_{ij}^{(12)}(\boldsymbol{p}_1; \boldsymbol{p}_2, \boldsymbol{p}_3) = C_{ji}^{(21)}(\boldsymbol{p}_1; \boldsymbol{p}_3, \boldsymbol{p}_2)$$
$$= -L_i^{(1)}(\boldsymbol{p}_2) L_j^{(2)}(\boldsymbol{p}_1, \boldsymbol{p}_2) P_{\mathrm{L}}(p_1) P_{\mathrm{L}}(p_2), \quad \text{(A36)}$$

$$C_{ijk}^{(112)}(\boldsymbol{p}_1, \boldsymbol{p}_2, \boldsymbol{p}_3) = C_{kij}^{(211)}(\boldsymbol{p}_3, \boldsymbol{p}_1, \boldsymbol{p}_2) = C_{jki}^{(121)}(\boldsymbol{p}_2, \boldsymbol{p}_3, \boldsymbol{p}_1)$$
$$= L_i^{(1)}(\boldsymbol{p}_1) L_j^{(1)}(\boldsymbol{p}_2) L_k^{(2)}(\boldsymbol{p}_1, \boldsymbol{p}_2) P_{\mathrm{L}}(p_1) P_{\mathrm{L}}(p_2). \quad \text{(A37)}$$

As in paper I, diagrammatic representations are helpful to understand the structure of perturbative terms. With Feynman
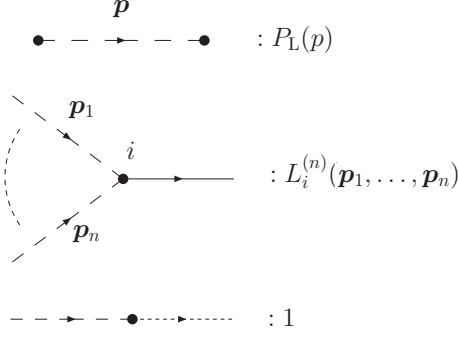
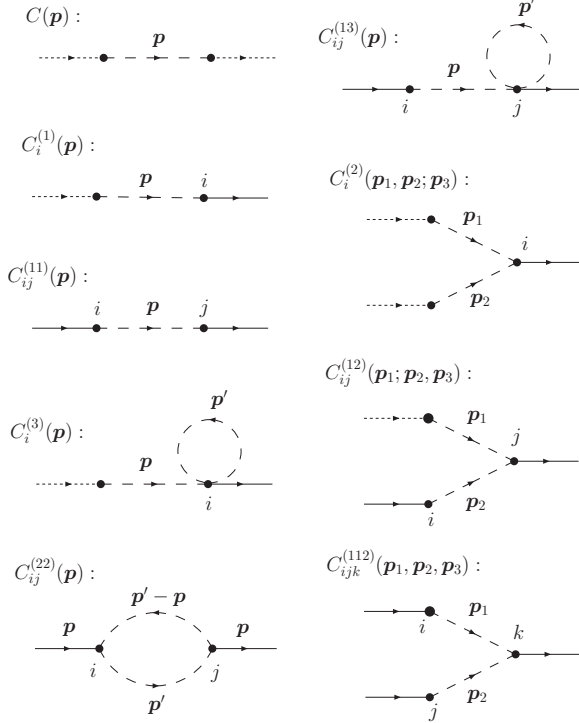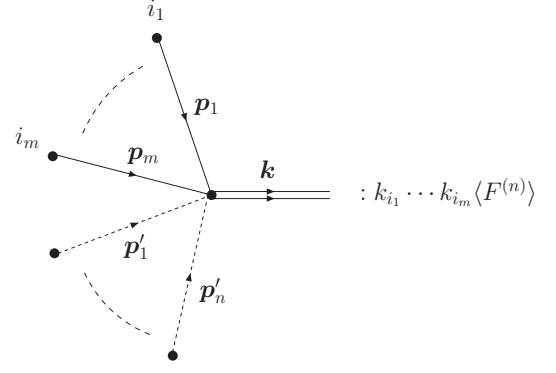FIG. 6: Feynman rules for diagrammatic representations.

FIG. 7: Diagrammatic representations of polyspectra.

FIG. 8: Feynman rules for external lines. The momentum conservation, $k = p_1 + \cdots p_m + p'_1 + \cdots p'_n$, is assumed.

of the nonlinear power spectrum in quasi-linear regime than the standard EPT. In the diagrammatic interpretation, the use of exponential prefactor corresponds to the partial renormalization of the vacuum graphs, as depicted in Fig. 10.

In real space, it is straightforward to evaluate Eq. (A11) using Eqs. (A12)–(A37) and perturbative kernels in real space, $L^{(n)}$. The above expressions are not confined in real space, and they are also applicable for redshift-space clustering when we use perturbative kernels $L^{s(n)}$ in Eqs. (A29)–(A37). As a result, the mixed polyspectra in redshift space are obtained from those in real space, subjecting to linear transformations:

$$C^{(n_1 \cdots n_m)}_{i_1 \cdots i_m} \rightarrow C^{s(n_1 \cdots n_m)}_{i_1 \cdots i_m} = R^{(n_1)}_{i_1 j_1} \cdots R^{(n_m)}_{i_m j_m} C^{(n_1 \cdots n_m)}_{j_1 \cdots j_m}. \quad \text{(A38)}$$

Therefore, it is desirable to first perform the integrations which appear in Eqs. (A12)–(A17) with decomposed polyspectra of Eqs. (A24)–(A27) in real space. The calculations are similar to those presented in Appendix A of paper I. Several integrations we need are already given there, and others are not. To present the results, we first define the following integrals:

$$Q_n(k) = \frac{k^3}{4\pi^2} \int_0^\infty dr\, P_L(kr)$$
$$\times \int_{-1}^1 dx P_L[k(1 + r^2 - 2rx)^{1/2}]\, \tilde{Q}_n(r, x), \quad \text{(A39)}$$

$$R_n(k) = \frac{k^3}{4\pi^2} P_L(k) \int_0^\infty dr\, P_L(kr)\, \tilde{R}_n(r), \quad \text{(A40)}$$

where

$$\tilde{Q}_1 = \frac{r^2(1 - x^2)^2}{(1 + r^2 - 2rx)^2}, \quad \tilde{Q}_2 = \frac{(1 - x^2)rx(1 - rx)}{(1 + r^2 - 2rx)^2}, \quad \text{(A41)}$$

$$\tilde{Q}_3 = \frac{x^2(1 - rx)^2}{(1 + r^2 - 2rx)^2}, \quad \tilde{Q}_4 = \frac{1 - x^2}{(1 + r^2 - 2rx)^2}, \quad \text{(A42)}$$

$$\tilde{Q}_5 = \frac{rx(1 - x^2)}{1 + r^2 - 2rx}, \quad \tilde{Q}_6 = \frac{(1 - 3rx)(1 - x^2)}{1 + r^2 - 2rx}, \quad \text{(A43)}$$

rules of Fig. 6 and appropriate statistical factors, Eqs. (A29)–(A37) are diagrammatically represented in Fig. 7. Substituting Eqs. (A12)–(A17) and (A24)–(A37) into Eq. (A11), we obtain a lengthy expression of $P_{obj}(k)$. For a diagrammatic representation of the result, we introduce additional Feynman rules for external lines in Fig. 8. All the contributions to the power spectrum $P_{obj}(k)$, but the exponential prefactor, are diagrammatically given in Fig. 9. In the exponent of the exponential prefactor in Eq. (A11), we consider only the first order in $P_L(k)$, since the remaining factor is already first order. In this approximation, the exponential factor corresponds to the bubble diagrams in Fig. 10. If we expand this exponential factor as well, we obtain a standard loop expansion of the power spectrum. In the absence of bias, the result agrees with that of standard EPT. In paper I, we pointed out that keeping the exponential prefactor unexpanded provides a better description
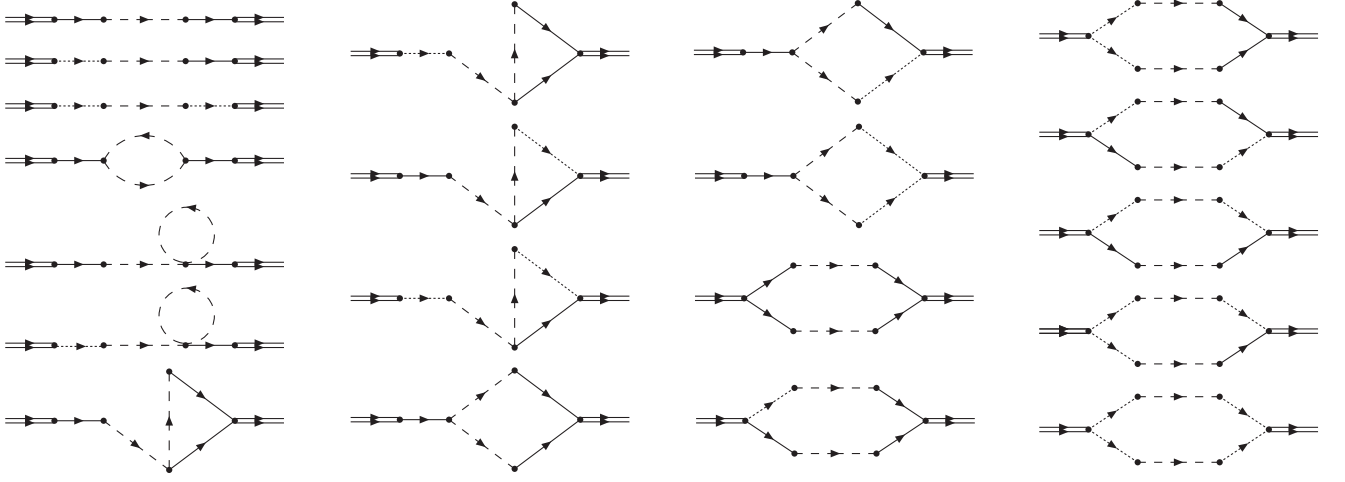
FIG. 9: All kinds of tree and one-loop diagrams for the biased power spectrum but an exponential prefactor. Topologically equivalent diagrams are not listed.
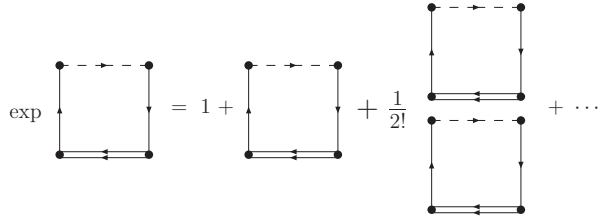

FIG. 10: Diagrammatic representation of the exponential prefactor in one-loop approximation.

$$\tilde{Q}_7 = \frac{x^2(1 - rx)}{1 + r^2 - 2rx}, \quad \tilde{Q}_8 = \frac{r^2(1 - x^2)}{1 + r^2 - 2rx}, \tag{A44}$$

$$\tilde{Q}_9 = \frac{rx(1 - rx)}{1 + r^2 - 2rx}, \quad \tilde{Q}_{10} = 1 - x^2, \tag{A45}$$

$$\tilde{Q}_{11} = x^2, \quad \tilde{Q}_{12} = rx, \quad \tilde{Q}_{13} = r^2, \tag{A46}$$

and

$$\tilde{R}_1 = \int_{-1}^{1} dx \frac{r^2(1 - x^2)^2}{1 + r^2 - 2rx}$$
$$= -\frac{1 + r^2}{24r^2}(3 - 14r^2 + 3r^4) + \frac{(r^2 - 1)^4}{16r^3} \ln \left| \frac{1 + r}{1 - r} \right|, \tag{A47}$$

$$\tilde{R}_2 = \int_{-1}^{1} dx \frac{(1 - x^2)rx(1 - rx)}{1 + r^2 - 2rx}$$
$$= \frac{1 - r^2}{24r^2}(3 - 2r^2 + 3r^4) + \frac{(r^2 - 1)^3(1 + r^2)}{16r^3} \ln \left| \frac{1 + r}{1 - r} \right|, \tag{A48}$$

After lengthy algebra (see also paper I), we obtain

$$C(\boldsymbol{k}) = P_{\mathrm{L}}(k), \tag{A49}$$

$$C_i^{(1)}(\boldsymbol{k}) = \frac{k_i}{k^2} P_{\mathrm{L}}(k), \tag{A50}$$

$$C_i^{(3)}(\boldsymbol{k}) = \frac{5}{21} \frac{k_i}{k^2} R_1(k), \tag{A51}$$

$$C_{ij}^{(11)}(\boldsymbol{k}) = -\frac{k_i k_j}{k^4} P_{\mathrm{L}}(k), \tag{A52}$$

$$C_{ij}^{(22)}(\boldsymbol{k}) = -\frac{9}{98} \frac{k_i k_j}{k^4} Q_1(k), \tag{A53}$$

$$C_{ij}^{(13)}(\boldsymbol{k}) = C_{ij}^{(31)}(\boldsymbol{k}) = -\frac{5}{21} \frac{k_i k_j}{k^4} R_1(k), \tag{A54}$$

$$\int \frac{d^3 p}{(2\pi)^3} C_i^{(2)}(\boldsymbol{k}, -\boldsymbol{p}; \boldsymbol{p} - \boldsymbol{k}) = \frac{3}{7} \frac{k_i}{k^2} [R_1(k) + R_2(k)], \tag{A55}$$

$$\int \frac{d^3 p}{(2\pi)^3} C_i^{(2)}(-\boldsymbol{p}, \boldsymbol{p} - \boldsymbol{k}; \boldsymbol{k}) = -\frac{3}{7} \frac{k_i}{k^2} Q_8(k), \tag{A56}$$

$$\int \frac{d^3 p}{(2\pi)^3} C_{ij}^{(12)}(\boldsymbol{k}; -\boldsymbol{p}, \boldsymbol{p} - \boldsymbol{k}) = \int \frac{d^3 p}{(2\pi)^3} C_{ij}^{(21)}(\boldsymbol{k}; -\boldsymbol{p}, \boldsymbol{p} - \boldsymbol{k})$$
$$= -\frac{3}{14} \frac{\delta_{ij}}{k^2} R_1(k) + \frac{3}{14} \frac{k_i k_j}{k^4} [R_1(k) + 2R_2(k)], \tag{A57}$$

$$\int \frac{d^3 p}{(2\pi)^3} C_{ij}^{(12)}(-\boldsymbol{p}; \boldsymbol{p} - \boldsymbol{k}, \boldsymbol{k}) = -\frac{3}{7} \frac{k_i k_j}{k^4} Q_5(k), \tag{A58}$$

$$\int \frac{d^3 p}{(2\pi)^3} C_{ij}^{(21)}(-\boldsymbol{p}; \boldsymbol{p} - \boldsymbol{k}, \boldsymbol{k}) = -\frac{3}{7} \frac{k_i k_j}{k^4} [R_1(k) + R_2(k)], \tag{A59}$$

$$\int \frac{d^3p}{(2\pi)^3} C_{ijk}^{(112)}(\boldsymbol{k}, -\boldsymbol{p}, \boldsymbol{p} - \boldsymbol{k}) = \int \frac{d^3p}{(2\pi)^3} C_{ijk}^{(121)}(\boldsymbol{k}, -\boldsymbol{p}, \boldsymbol{p} - \boldsymbol{k})$$

$$= \frac{3}{14} \frac{k_i \delta_{jk}}{k^4} R_1(k) - \frac{3}{14} \frac{k_i k_j k_k}{k^6} [R_1(k) + 2R_2(k)], \quad \text{(A60)}$$

$$\int \frac{d^3p}{(2\pi)^3} C_{ijk}^{(211)}(\boldsymbol{k}, -\boldsymbol{p}, \boldsymbol{p} - \boldsymbol{k})$$

$$= \frac{3}{14} \frac{k_i \delta_{jk}}{k^4} Q_1(k) - \frac{3}{14} \frac{k_i k_j k_k}{k^6} [Q_1(k) + 2Q_2(k)], \quad \text{(A61)}$$

$$\int \frac{d^3p}{(2\pi)^3} C(\boldsymbol{p}) C(\boldsymbol{k} - \boldsymbol{p}) = Q_{13}(k), \quad \text{(A62)}$$

$$\int \frac{d^3p}{(2\pi)^3} C(\boldsymbol{p}) C_i^{(1)}(\boldsymbol{k} - \boldsymbol{p}) = \frac{k_i}{k^2} Q_{12}(k), \quad \text{(A63)}$$

$$\int \frac{d^3p}{(2\pi)^3} C(\boldsymbol{p}) C_{ij}^{(11)}(\boldsymbol{k} - \boldsymbol{p})$$

$$= -\frac{1}{2} \frac{\delta_{ij}}{k^2} Q_{10}(k) + \frac{1}{2} \frac{k_i k_j}{k^4} [Q_{10}(k) - 2Q_{11}(k)], \quad \text{(A64)}$$

$$\int \frac{d^3p}{(2\pi)^3} C_i^{(1)}(\boldsymbol{p}) C_j^{(1)}(\boldsymbol{k} - \boldsymbol{p})$$

$$= -\frac{1}{2} \frac{\delta_{ij}}{k^2} Q_8(k) + \frac{1}{2} \frac{k_i k_j}{k^4} [Q_8(k) + 2Q_9(k)], \quad \text{(A65)}$$

$$\int \frac{d^3p}{(2\pi)^3} C_{(i}^{(1)}(\boldsymbol{p}) C_{jk)}^{(11)}(\boldsymbol{k} - \boldsymbol{p})$$

$$= -\frac{1}{2} \frac{\delta_{(ij} k_{k)}}{k^4} Q_6(k) + \frac{1}{2} \frac{k_i k_j k_k}{k^6} [Q_6(k) - 2Q_7(k)], \quad \text{(A66)}$$

$$\int \frac{d^3p}{(2\pi)^3} C_{(ij}^{(11)}(\boldsymbol{p}) C_{kl)}^{(11)}(\boldsymbol{k} - \boldsymbol{p}) = \frac{3}{8} \frac{\delta_{(ij} \delta_{kl)}}{k^4} Q_1(k)$$

$$- \frac{1}{4} \frac{\delta_{(ij} k_k k_{l)}}{k^6} [3Q_1(k) + 12Q_2(k) - 2Q_4(k)]$$

$$+ \frac{1}{8} \frac{k_i k_j k_k k_l}{k^8} [3Q_1(k) + 24Q_2(k) + 8Q_3(k) - 4Q_4(k)], \quad \text{(A67)}$$

where the spatial indices are symmetrized over in Eqs. (A66) and (A67). In deriving the above equations, the transverse part of Eq. (A5) does not contribute at all, because the rotational covariance implies

$$\int \frac{d^3p}{(2\pi)^3} g(\boldsymbol{k}, \boldsymbol{p}) \boldsymbol{T}(\boldsymbol{k}, -\boldsymbol{p}, \boldsymbol{p}) \propto \boldsymbol{k}, \quad \text{(A68)}$$

where g is a scalar function.

Applying the transformation of Eq. (A38), the corresponding integrals in redshift space are straightforwardly obtained. The resulting integrals are substituted in Eqs. (A11)–(A17)

with the help of Eq. (A24)–(A27). The final result is represented as

$$P_{\text{obj}}^{(s)}(\boldsymbol{k}) = \exp\left\{-\left[1 + f(f+2)\mu^2\right](k/k_{\text{NL}})^2\right\}$$

$$\times \left[\left(1 + \langle F' \rangle + f\mu^2\right)^2 P_{\text{L}}(k) + \sum_{n,m} \mu^{2n} f^m E_{nm}(k)\right], \quad \text{(A69)}$$

where

$$k_{\text{NL}} = \left[\frac{1}{6\pi^2} \int dk P_{\text{L}}(k)\right]^{-1/2}, \quad \text{(A70)}$$

and

$$E_{00} = \frac{9}{98} Q_1 + \frac{3}{7} Q_2 + \frac{1}{2} Q_3 + \frac{10}{21} R_1 + \frac{6}{7} R_2$$

$$+ \langle F' \rangle \left(\frac{6}{7} Q_5 + 2Q_7 + \frac{4}{3} R_1 + \frac{12}{7} R_2\right)$$

$$+ \langle F'' \rangle \left(\frac{3}{7} Q_8 + Q_9\right) + \langle F' \rangle^2 \left(Q_9 + Q_{11} + \frac{6}{7} R_1 + \frac{6}{7} R_2\right)$$

$$+ 2\langle F' \rangle \langle F'' \rangle Q_{12} + \frac{1}{2} \langle F'' \rangle^2 Q_{13}, \quad \text{(A71)}$$

$$E_{11} = \frac{18}{49} Q_1 + \frac{12}{7} Q_2 + 2Q_3 + \frac{40}{21} R_1 + \frac{24}{7} R_2$$

$$+ \langle F' \rangle \left(\frac{18}{7} Q_5 + 6Q_7 + 4R_1 + \frac{36}{7} R_2\right)$$

$$+ \langle F'' \rangle \left(\frac{6}{7} Q_8 + 2Q_9\right)$$

$$+ \langle F' \rangle^2 \left(2Q_9 + 2Q_{11} + \frac{12}{7} R_1 + \frac{12}{7} R_2\right)$$

$$+ 2\langle F' \rangle \langle F'' \rangle Q_{12}, \quad \text{(A72)}$$

$$E_{12} = -\frac{3}{14} Q_1 - \frac{3}{2} Q_2 + \frac{1}{4} Q_4 - \frac{6}{7} R_1 + \langle F' \rangle \left(Q_6 - \frac{6}{7} R_1\right)$$

$$- \frac{1}{2} \langle F'' \rangle Q_8 - \frac{1}{2} \langle F' \rangle^2 (Q_8 - Q_{10}), \quad \text{(A73)}$$

$$E_{22} = \frac{57}{98} Q_1 + \frac{51}{14} Q_2 + 3Q_3 - \frac{1}{4} Q_4 + \frac{16}{7} R_1 + \frac{30}{7} R_2$$

$$+ \langle F' \rangle \left(\frac{12}{7} Q_5 - Q_6 + 6Q_7 + \frac{18}{7} R_1 + \frac{24}{7} R_2\right)$$

$$+ \langle F'' \rangle \left(\frac{1}{2} Q_8 + Q_9\right)$$

$$+ \langle F' \rangle^2 \left(\frac{1}{2} Q_8 + Q_9 - \frac{1}{2} Q_{10} + Q_{11}\right), \quad \text{(A74)}$$

$$E_{23} = -\frac{3}{7} Q_1 - 3Q_2 + \frac{1}{2} Q_4 - \frac{6}{7} R_1 + \langle F' \rangle Q_6, \quad \text{(A75)}$$

$$E_{24} = \frac{3}{16} Q_1, \quad \text{(A76)}$$

$$E_{33} = \frac{3}{7}Q_1 + \frac{27}{7}Q_2 + 2Q_3 - \frac{1}{2}Q_4 + \frac{6}{7}R_1 + \frac{12}{7}R_2$$
$$+ \langle F' \rangle (-Q_6 + 2Q_7), \tag{A77}$$

$$E_{34} = -\frac{3}{8}Q_1 - \frac{3}{2}Q_2 + \frac{1}{4}Q_4, \tag{A78}$$

$$E_{44} = \frac{3}{16}Q_1 + \frac{3}{2}Q_2 + \frac{1}{2}Q_3 - \frac{1}{4}Q_4, \tag{A79}$$

and all the other E_{nm} which are not listed above are zero.

Equations (A69)–(A79), together with Eqs. (A39)–(A48), are complete set of equations to give the general one-loop power spectrum with effects of local Lagrangian bias and redshift-space distortions. Although the number of terms are large, they are all given by simple integrals of $Q_n(k)$ and $R_n(k)$ of Eqs. (A39) and (A40), which are numerically easy to evaluate. The power spectrum in real space is obtained by simply putting $f = 0$. When the bias is not present, $\langle F' \rangle = \langle F'' \rangle = 0$, this result exactly agrees with the one which is derived in paper I. A cross power spectrum is obtained by substitutions of Eqs. (A18)–(A22), after expanding Eq. (A69) in terms of $\langle F' \rangle$ and $\langle F'' \rangle$.

[1] P. J. E. Peebles and J. T. Yu, Astrophys. J. **162**, 815 (1970); R. A. Sunyaev and Y. B. Zel'dovich, Astrophys. Space Sci.**7**, 3 (1970); J. R. Bond and G. Efstathiou, Astrophys. J. Letters, **285**, L45 (1984); J. R. Bond and G. Efstathiou, Mon. Not. R. Astron. Soc., **226**, 655 (1987); J. A. Holtzman, Astrophys. J. Suppl. Ser., **71**, 1 (1989).

[2] A. D. Miller et al., Astrophys. J. Letters, **524**, L1 (1999); P. de Bernardis et al., Nature (London) , **404**, 955 (2000); S. Hanany et al., Astrophys. J. Letters, 545, L5 (2000); C. L. Bennett et al., Astrophys. J. Suppl. Ser., **148**, 1 (2003).

[3] D. J. Eisenstein, W. Hu, and M. Tegmark, Astrophys. J. Letters, **504**, L57 (1998); A. Cooray, W. Hu, D. Huterer, and M. Joffre, Astrophys. J. Letters, **557**, L7 (2001).

[4] C. Alcock and B. Paczynski, Nature (London) , **281**, 358 (1979).

[5] W. E. Ballinger, J. A. Peacock, and A. F. Heavens, Mon. Not. R. Astron. Soc., **282**, 877 (1996); T. Matsubara and Y. Suto, Astrophys. J. Letters, **470**, L1 (1996).

[6] T. Matsubara and A. S. Szalay, Astrophys. J. Letters, **556**, L67 (2001); T. Matsubara and A. S. Szalay, Astrophys. J. , **574**, 1 (2002); T. Matsubara and A. S. Szalay, Phys. Rev. Lett. , **90**, 021302(2003).

[7] W. Hu and Z. Haiman, Phys. Rev. D , **68**, 063004 (2003); C. Blake and K. Glazebrook, Astrophys. J. , **594**, 665 (2003); H.-J. Seo and D. J. Eisenstein, Astrophys. J. , **598**, 720 (2003); E. V. Linder, Phys. Rev. D , **68**, 083504 (2003); L. Amendola, C. Quercellini, and E. Giallongo, Mon. Not. R. Astron. Soc., **357**, 429 (2005); C. Blake and S. Bridle, Mon. Not. R. Astron. Soc., **363**, 1329 (2005); K. Glazebrook and C. Blake, Astrophys. J. , **631**, 1 (2005); D. Dolney, B. Jain, and M. Takada, Mon. Not. R. Astron. Soc., **366**, 884 (2006); H.-J. Seo and D. J. Eisenstein, Astrophys. J. , **665**, 14 (2007).

[8] T. Matsubara, Astrophys. J. , **615**, 573 (2004).

[9] D. J. Eisenstein et al., Astrophys. J. **633**, 560 (2005); S. Cole et al., Mon. Not. R. Astron. Soc., **362**, 505 (2005); M. Tegmark et al., Phys. Rev. D **74**, 123507 (2006); G. Hütsi, Astron. Astrophys., **449**, 891 (2006); W. Percival et al., Astrophys. J. **657**, 51 (2007); N. Padmanabhan et al. Mon. Not. R. Astron. Soc., 378, 852 (2007); T. Okumura, T. Matsubara, D. J. Eisenstein, I. Kayo, C. Hikage, C., A. S. Szalay, and D. P. Schneider, Astrophys. J. , **676**, 889 (2008); J. Estrada, E. Sefusatti, and J. A. Frieman, arXiv:0801.3485.

[10] H.-J. Seo and D. J. Eisenstein, Astrophys. J. , **633**, 575 (2005); V. Springel, et al., Nature (London) , **435**, 629 (2005); J. Guzik, G. Bernstein, and R. E. Smith, Mon. Not. R. Astron. Soc., **375**, 1329 (2007); Z. Ma, Astrophys. J. , , **665**, 887 (2007); R. E. Smith, R. Scoccimarro, and R. K. Sheth, Phys. Rev. D , **77**, 043525 (2008); R. Angulo, C. M. Baugh, C. S. Frenk, & C. G. Lacey, Mon. Not. R. Astron. Soc., **383**, 755 (2008).

[11] A. Meiksin, M. White, and J. A. Peacock, Mon. Not. R. Astron. Soc., **304**, 851 (1999); M. White, Astroparticle Physics, **24**, 334 (2005); A. E. Schulz and M. White, Astroparticle Physics, **25**, 172 (2006); E. Huff, A. E. Schulz, M. White, D. J. Schlegel, and M. S. Warren, Astroparticle Physics, **26**, 351 (2007); D. J. Eisenstein, H.-J. Seo, E. Sirko, and D. N. Spergel, Astrophys. J. , **664**, 675 (2007); T. Nishimichi, et al., Publ. Astron. Soc. Japan, **59**, 1049 (2007).

[12] D. J. Eisenstein, H.-J. Seo, and M. White, Astrophys. J. , **664**, 660 (2007).

[13] R. Angulo, C. M. Baugh, C. S. Frenk, R. G. Bower, A. Jenkins, & S. L. Morris, Mon. Not. R. Astron. Soc., **362**, L25 (2005).

[14] A. G. Sanchez, C. M. Baugh, and R. Angulo, arXiv:0804.0233.

[15] N. Kaiser, Astrophys. J. Letters, **284**, L9 (1984); M. Davis, G. Efstathiou, C. S. Frenk, and S. D. M. White, Astrophys. J. , **292**, 371 (1985).

[16] J. Bardeen, J. R. Bond, N. Kaiser, and A. S. Szalay, Astrophys. J. , **304**, 15 (1986).

[17] J. C. Jackson, Mon. Not. R. Astron. Soc., **156**, 1P (1972); W. L. W. Sargent and E. L. Turner, Astrophys. J. Letters, **212**, L3 (1977).

[18] N. Kaiser, Mon. Not. R. Astron. Soc., **227**, 1 (1987).

[19] P. Coles, Mon. Not. R. Astron. Soc., **262**, 1065 (1993); J. N. Fry and E. Gaztanaga, Astrophys. J. , **413**, 447 (1993); T. Matsubara, Astrophys. J. , **525**, 543 (1999).

[20] R. J. Scherrer and D. H. Weinberg, Astrophys. J. , **504**, 607 (1998)

[21] R. Scoccimarro, Phys. Rev. D , **70**, 083007 (2004).

[22] R. Juszkiewicz, Mon. Not. R. Astron. Soc., **197**, 931 (1981); E. T. Vishniac, Mon. Not. R. Astron. Soc., **203**, 345 (1983); J. N. Fry, Astrophys. J. , **279**, 499 (1984); B. Jain and E. Bertschinger, Astrophys. J. , **431**, 495 (1994).

[23] M. H. Goroff, B. Grinstein, S.-J. Rey, and M. B. Wise, Astrophys. J. , **311**, 6 (1986); R. Scoccimarro and J. A. Frieman, Astrophys. J. Suppl. Ser., **105**, 37 (1996); R. Scoccimarro and J. A. Frieman, Astrophys. J. , **473**, 620 (1996).

[24] Y. Suto, M. Sasaki, Phys. Rev. Lett. , **66**, 264 (1991); N. Makino, M. Sasaki, and Y. Suto, Phys. Rev. D , **46**, 585 (1992).

[25] F. Bernardeau, S. Colombi, E. Gaztañaga, and R. Scoccimarro, Phys. Rep., **367**, 1 (2002).

[26] J. N. Fry and E. Gaztanaga, Astrophys. J. , **413**, 447 (1993).

[27] A. F. Heavens, S. Matarrese, and L. Verde, Mon. Not. R. Astron. Soc., **301**, 797 (1998).

[28] A. Taruya, Astrophys. J. , **537**, 37 (2000).

[29] P. McDonald, Phys. Rev. D , **74**, 103512 (2006); P. McDonald, Phys. Rev. D , **74**, 129901(E) (2006); P. McDonald, arXiv:0806.1061.

[30] R. E. Smith, R. Scoccimarro, and R. K. Sheth, Phys. Rev. D , **75**, 063512 (2007); R. E. Smith, R. K. Sheth, and R. Scoccimarro, Phys. Rev. D , **78**, 023523 (2008).

[31] R. Scoccimarro, H. M. P. Couchman, and J. A. Frieman, Astrophys. J. , **517**, 531 (1999).

[32] D. Jeong and E. Komatsu, arXiv:0805.2632.

[33] H. J. Mo and S. D. M. White, Mon. Not. R. Astron. Soc., **282**, 347 (1996).

[34] H. J. Mo, Y. P. Jing, and S. D. M. White, Mon. Not. R. Astron. Soc., **284**, 189 (1997).

[35] R. K. Sheth and G. Lemson, Mon. Not. R. Astron. Soc., **304**, 767 (1999).

[36] R. K. Sheth and G. Tormen, Mon. Not. R. Astron. Soc., **308**, 119 (1999).

[37] U. Seljak, Mon. Not. R. Astron. Soc., **318**, 203 (2000).

[38] J. A. Peacock and R. E. Smith, Mon. Not. R. Astron. Soc., **318**, 1144 (2000).

[39] C.-P. Ma and J. N. Fry, Astrophys. J. , **543**, 503 (2000).

[40] R. Scoccimarro, R. K. Sheth, L. Hui, and B. Jain, Astrophys. J. , **546**, 20 (2001).

[41] A. Cooray and R. Sheth, Phys. Rep., **372**, 1 (2002).

[42] W. H. Press and P. Schechter, Astrophys. J. , **187**, 425 (1974).

[43] R. I. Epstein, Mon. Not. R. Astron. Soc., **205**, 207 (1983); J. A. Peacock and A. F. Heavens, Mon. Not. R. Astron. Soc., **243**, 133 (1990); R. G. Bower, Mon. Not. R. Astron. Soc., **248**, 332 (1991); J. R. Bond, S. Cole, G. Efstathiou, and N. Kaiser, Astrophys. J. , **379**, 440 (1991).

[44] R. J. Scherrer and E. Bertschinger, Astrophys. J. , **381**, 349 (1991).

[45] S. D. M. White and M. J. Rees, Mon. Not. R. Astron. Soc., **183**, 341 (1978); S. D. M. White and C. S. Frenk, Astrophys. J. , **379**, 52 (1991); G. Kauffmann, J. M. Colberg, A. Diaferio, and S. D. M. White, Mon. Not. R. Astron. Soc., **303**, 188 (1999); A. J. Benson, S. Cole, C. S. Frenk, C. M. Baugh, and C. G. Lacey, Mon. Not. R. Astron. Soc., **311**, 793 (2000).

[46] T. Buchert, Astron. Astrophys., **223**, 9 (1989); F. Moutarde, J.-M. Alimi, F. R. Bouchet, R. Pellat, and A. Ramani, Astrophys. J. , **382**, 377 (1991); T. Buchert, Mon. Not. R. Astron. Soc., **254**, 729 (1992); T. Buchert and J. Ehlers, Mon. Not. R. Astron. Soc., **264**, 375 (1993); T. Buchert, Mon. Not. R. Astron. Soc., **267**, 811 (1994); E. Hivon, F. R. Bouchet, S. Colombi and R. Juszkiewicz, Astron. Astrophys., **298**, 643 (1995); J. Ehlers and T. Buchert, General Relativity and Gravitation, **29**, 733 (1997); T. Tatekawa, Recent Res. Devel. Astrophys. **2** 1 (2005) (arXiv:astro-ph/0412025)

[47] P. Catelan, F. Lucchin, S. Matarrese, and C. Porciani, Mon. Not. R. Astron. Soc., **297**, 692 (1998); P. Catelan, S. Matarrese, and C. Porciani, Astrophys. J. Letters, **502**, L1 (1998).

[48] T. Matsubara, Phys. Rev. D , **77**, 063530 (2008) (paper I).

[49] R. Scoccimarro, Ann. N.Y. Acad. Sci. **927**, 13 (2001); M. Crocce and R. Scoccimarro, Phys. Rev. D , **73**, 063519 (2006); M. Crocce and R. Scoccimarro, Phys. Rev. D , **77**, 023533 (2008); P. Valageas, Astron. Astrophys., **465**, 725 (2007); S. Matarrese and M. Pietroni, Mod. Phys. Lett. A, **23**, 25 (2008); S. Matarrese and M. Pietroni, J. Cosmol. Astropart. Phys., 0706 (2007) 026; K. Izumi and J. Soda, Phys. Rev. D **76**, 083517 (2007); O. J. Rosten, J. Cosmol. Astropart. Phys., 01 (2008) 029; A. Taruya and T. Hiramatsu, Astrophys. J. , **674**, 617 (2008); M. Pietroni, arXiv:0806.0971; F. Bernardeau, M. Crocce, and R. Scoccimarro, arXiv:0806.2334.

[50] P. Valageas, Astron. Astrophys., **421**, 23 (2004); P. McDonald, Phys. Rev. D , **75**, 043514 (2007).

[51] S. Cole and N. Kaiser, Mon. Not. R. Astron. Soc., **237**, 1127 (1989).

[52] J. R. Bond and H. M. P. Couchman, in *Proceedings of the 2nd Canadian Conference on General Relativity and Relativistic Astrophysics* (World Scientific, Singapore, 1988), p. 385; A. N. Taylor, in *Cosmic Velocity Fields, Proceedings of the 9th IAP Astrophysics Meeting, Institut d'Astrophysique, Paris, July 12-17, 1993* (Editions Frontieres, Gif-sur-Yvette, 1993), p. 585; A. N. Taylor and A. J. S. Hamilton, Mon. Not. R. Astron. Soc., **282**, 767 (1996).

[53] S.-K. Ma, *Statistical Mechanics* (World Scientific, Singapore, 1985), Sec. 12

[54] F. R. Bouchet, S. Colombi, E. Hivon, and R. Juszkiewicz, Astron. Astrophys., **296**, 575 (1995); T. Matsubara, Progress of Theoretical Physics, **94**, 1151 (1995).

[55] T. Matsubara, Astrophys. J. , **535**, 1 (2000).

[56] C. Lacey and S. Cole, Mon. Not. R. Astron. Soc., **262**, 627 (1993); V. R. Eke, S. Cole, and C. S. Frenk, Mon. Not. R. Astron. Soc., **282**, 263 (1996); J. F. Navarro, C. S. Frenk, and S. D. M. White, Astrophys. J. , **490**, 493 (1997); E. L. Łokas and Y. Hoffman, in Proceedings of the Third International Workshop on the Identification of Dark Matter, ed. N.J.C. Spooner and V. Kudryavtsev (World Scientific, Singapore, 2001), arXiv:astro-ph/0011295.

[57] A. Lewis, A. Challinor, and A. Lasenby, Astrophys. J. **538**, 473 (2000).

[58] D. J. Eisenstein and W. Hu, Astrophys. J. , **511**, 5 (1999).

[59] H.-J. Seo, E. R. Siegel, D. J. Eisenstein, and M. White, arXiv:0805.0117.

[60] V. Desjacques, arXiv:0806.0007.

[61] F. Bernardeau and P. Valageas, Phys. Rev. D , **78** 083503 (2008).

[62] M. White, Mon. Not. R. Astron. Soc., **321**, 1 (2001); U. Seljak, Mon. Not. R. Astron. Soc., **325**, 1359 (2001); X. Kang, Y. P. Jing, H. J. Mo, G. Börner, Mon. Not. R. Astron. Soc., **336**, 892 (2002); A. Cooray, Mon. Not. R. Astron. Soc., **348**, 250 (2004); R. Skibba, R. K. Sheth, A. J. Connolly, and R. Scranton, Mon. Not. R. Astron. Soc., **369**, 68 (2006); A. Slosar, U. Seljak, and A. Tasitsiomi, Mon. Not. R. Astron. Soc., **366**, 1455 (2006); J. L. Tinker, Mon. Not. R. Astron. Soc., **374**, 477 (2007).

[63] Ya. B. Zel'dovich, Astron. Astrophys., **5**, 84 (1970).

[64] P. Catelan, Mon. Not. R. Astron. Soc., **276**, 115 (1995); P. Catelan and T. Theuns, Mon. Not. R. Astron. Soc., **282**, 455 (1996).